C IV emission-line properties and systematic trends in quasar black hole mass estimates

Liam Coatman,[1]⋆ Paul C. Hewett,[1] Manda Banerji[1] and Gordon T. Richards[2]

[1]*Institute of Astronomy, Madingley Road, Cambridge CB3 0HA, UK*
[2]*Department of Physics, Drexel University, 3141 Chestnut Street, Philadelphia PA 19104, USA*

ABSTRACT

Black hole masses are crucial to understanding the physics of the connection between quasars and their host galaxies and measuring cosmic black hole-growth. At high redshift, $z \gtrsim 2.1$, black hole masses are normally derived using the velocity width of the C IV $\lambda\lambda$1548, 1550 broad emission line, based on the assumption that the observed velocity widths arise from virial-induced motions. In many quasars, the C IV emission line exhibits significant blue asymmetries ('blueshifts') with the line centroid displaced by up to thousands of km s^{-1} to the blue. These blueshifts almost certainly signal the presence of strong outflows, most likely originating in a disc wind. We have obtained near-infrared spectra, including the Hα λ6565 emission line, for 19 luminous ($L_{Bol} = 46.5$–47.5 erg s^{-1}) Sloan Digital Sky Survey quasars, at redshifts $2 < z < 2.7$, with C IV emission lines spanning the full range of blueshifts present in the population. A strong correlation between C IV velocity width and blueshift is found and, at large blueshifts, >2000 km s^{-1}, the velocity widths appear to be dominated by non-virial motions. Black hole masses, based on the full width at half-maximum of the C IV emission line, can be overestimated by a factor of 5 at large blueshifts. A larger sample of quasar spectra with both C IV and H β, or Hα, emission lines will allow quantitative corrections to C IV-based black hole masses as a function of blueshift to be derived. We find that quasars with large C IV blueshifts possess high Eddington luminosity ratios and that the fraction of high-blueshift quasars in a flux-limited sample is enhanced by a factor of approximately 4 relative to a sample limited by black hole mass.

Key words: galaxies: evolution.

1 INTRODUCTION

Supermassive black holes (BHs) are found at the centres of most nearby massive galaxies and the BH mass and mass of the host galaxy spheroid are strongly correlated (Ferrarese & Merritt 2000; Gebhardt et al. 2000; Kormendy & Ho 2013). Although any underlying causal mechanism(s) responsible for the correlation is yet to be conclusively identified, there is considerable observational and theoretical support for models that involve BH-fuelling, outflows and a 'feedback' relationship (e.g. King & Pounds 2015). The number density of quasars, which evolves strongly with redshift, peaks at redshifts $2 \lesssim z \lesssim 3$ (e.g. Brandt & Hasinger 2005; Richards et al. 2006a) and the most massive ($M_{BH} \gtrsim 10^9\,M_\odot$) present-day BHs experienced much of their growth during this epoch. The star formation rate, which closely follows the cosmological evolution of the quasar luminosity function, also peaks during this epoch (e.g. Boyle & Terlevich 1998). Quantifying the growth rate of massive BHs at

$2 \lesssim z \lesssim 3$ would therefore help significantly in understanding the role quasars play in galaxy evolution.

Reliable estimates of BH masses are a pre-requisite for investigating the relationship between BHs and their host galaxies. If the line-emitting clouds in the broad-line region (BLR) are assumed to be virialized and moving in a potential dominated by the central BH, then the BH mass is simply a product of the BLR size and the square of the virial velocity. The reverberation-mapping technique uses the time lag between variations in the continuum emission and correlated variations in the broad-line emission to measure the typical size of the BLR (Peterson 1993, 2014). The full width at half-maximum (FWHM) or dispersion (σ; derived from the second moment) velocity of the prominent broad emission line of H β (4862.7 Å)[1] is used as an indicator of the virial velocity, with extensions to other low-ionization emission lines such as Hα (6564.6 Å) and Mg II$\lambda\lambda$2796.4, 2803.5 (e.g. McLure & Jarvis 2002; Vestergaard 2002; Wu et al. 2004; Kollmeier et al. 2006; Onken & Kollmeier 2008; Wang et al.

⋆ E-mail: lc585@ast.cam.ac.uk

[1] Vacuum wavelengths are employed throughout the paper.

2009; Rafiee & Hall 2011). Extensive reverberation-mapping campaigns have provided accurate BH masses for ∼50 active galactic nuclei (AGN) at relatively low redshifts and of modest luminosity (e.g. Kaspi et al. 2000, 2007; Peterson et al. 2004; Bentz et al. 2009; Denney et al. 2010).

Reverberation-mapping campaigns have also revealed a tight relationship between the radius of the BLR and the quasar optical [or ultraviolet (UV)] luminosity (the *R–L* relation; e.g. Kaspi et al. 2000, 2007). This relation provides a much less expensive method of measuring the BLR radius, and large-scale studies of AGN and quasar demographics have thus become possible through the calibration of single-epoch virial-mass estimators using the reverberation-derived BH masses (e.g. Greene & Ho 2005; Vestergaard & Peterson 2006; Vestergaard & Osmer 2009; Shen et al. 2011; Shen & Liu 2012; Trakhtenbrot & Netzer 2012). The uncertainties in reverberation-mapped BH masses are estimated to be ∼0.4 dex (e.g. Peterson 2010), and the uncertainties in virial masses are similar (e.g. Vestergaard & Peterson 2006). Since the structure and geometry of the BLR is unknown, a virial coefficient f is introduced to transform the observed line-of-sight velocity inferred from the linewidth into a virial velocity. This simplification accounts for a significant part of the uncertainty in virial BH masses (in addition to, for example, describing the BLR with a single radius R and scatter in the *R–L* relation; Shen 2013). Furthermore, if the BLR is anisotropic (for example, in a flattened disc; e.g. Jarvis & McLure 2006) then the linewidth will be orientation-dependent (e.g. Runnoe et al. 2013a; Shen & Ho 2014; Brotherton et al. 2015).

At redshifts of $z \gtrsim 2.0$, the low-ionization hydrogen and Mg II emission lines are no longer present in the optical spectra of quasars and it is necessary to employ an emission line in the rest-frame UV. The strong C IV λλ1548.2, 1550.8 emission doublet is visible in the optical spectra of quasars to redshifts of $z \sim 5$ and C IV-derived BH masses have become the standard (e.g. Vestergaard & Peterson 2006; Park et al. 2013) for both individual quasars and in studies of quasar population demographics.

The luminosities of quasars at redshifts $z \gtrsim 2$ are much greater than the majority of AGN at lower redshifts for which reverberation-mapping results are available. Therefore, the reliability of the existing calibration involving C IV FWHM velocity measurements and UV luminosity is not established definitively when extrapolating to high redshifts and luminosities. While some authors have found good agreement between BH mass estimates based on C IV and H β (e.g. Vestergaard & Peterson 2006; Assef et al. 2011; Tilton & Shull 2013), others have questioned the consistency (e.g. Baskin & Laor 2005; Shen & Liu 2012; Trakhtenbrot & Netzer 2012).

Denney (2012) presented evidence that the interpretation of the FWHM velocity of the C IV emission being due primarily to virial motions within the quasar BLR requires care. Specifically, both a low-velocity core component and a blue excess to the C IV emission, both of which do not reverberate, can be present and Denney (2012) proposes that a contribution from an accretion disc wind or from a more distant narrow emission-line region is important.

Certainly, in contrast to the hydrogen Balmer lines and Mg II, the C IV emission line in quasar spectra exhibits a broad range of line shapes, including significant asymmetry, with shifts of the line-centroid to the blue ('blueshifts') of up to several thousand km s^{-1} (Richards et al. 2002; Baskin & Laor 2005; Sulentic et al. 2006). Shen & Liu (2012) found, using a sample of 60 luminous quasars, that the scatter between the FWHM of C IV and H β was correlated with the blueshift of C IV relative to H β. Shen et al. (2008) found a similar result by comparing C IV with Mg II for quasars from Sloan Digital Sky Survey (SDSS) DR5. The blueshifting of C IV is

usually interpreted as evidence for strong outflows (e.g. Sulentic et al. 2007; Richards et al. 2011) which, most likely, result from the presence of a radiation line-driven accretion-disc wind (e.g. Konigl & Kartje 1994; Murray et al. 1995; Proga, Stone & Kallman 2000; Everett 2005; Gallagher et al. 2015). In this picture, the non-virial wind component makes a significant contribution to the observed C IV-emission FWHM in quasars with large C IV blueshifts ('wind-dominated quasars') and hence increases the inferred BH masses. A primary goal of this paper is to present the full range of C IV emission-line blueshifts present among high-luminosity quasars at redshifts $z \sim 2.5$ and investigate potential systematic trends in the derived C IV-based BH masses as a function of blueshift.

Changes in the C IV blueshift and equivalent width (EW) are correlated with changes in the velocity widths and strengths of other optical and UV emission lines. In the spectra of lower redshift AGN, the FWHM of the broad H β emission line and the relative strengths of optical Fe II and H β have been identified as the features responsible for the largest variance in the population. These parameters form part of 'Eigenvector 1' (EV1), the first eigenvector in a principal component analysis which originated from the work of Boroson & Green (1992). The underlying driver behind EV1 is thought to be the Eddington ratio (e.g. Sulentic et al. 2000b; Shen & Ho 2014). Sulentic, Marziani & Dultzin-Hacyan (2000a) proposed a two-population model to classify AGN by their EV1 properties. In this scheme, AGN with FWHM(H β) < 4000 km s^{-1} and FWHM(H β) > 4000 km s^{-1} are classified as population A and B objects, respectively, although there is a continuous distribution of parameter values across this divide. Sulentic et al. (2007) added a measure of the C IV asymmetry to EV1, and found a strong association between blue-asymmetry and their population A quasars.

Denney (2012) found the level of contamination in single-epoch spectra from non-reverberating gas to be correlated with the shape (FWHM/σ) of the C IV profile. Runnoe et al. (2013b) found the scatter between the C IV and H β linewidths to be correlated with the continuum-subtracted peak flux ratio of the UV emission-line blend of Si IV+O IV (at 1400 Å) to that of C IV. Both authors used these correlations to propose empirical corrections to the C IV linewidth which can improve the consistency between C IV and H β-based virial BH mass estimates. In fact, the shape, peak flux relative to the 1400 Å blend, and blueshift of C IV , all correlate with one another and with other parameters in EV1. Therefore, EV1 provides a useful context for understanding systematic trends in C IV velocity widths, and hence virial BH masses.

Currently, the number of reverberation-mapped quasars is both small (∼50 quasars; Park et al. 2013) and, as highlighted by Richards et al. (2011), includes a restricted range of the C IV emission-line shapes seen in the quasar population. In particular, the reverberation-mapped objects generally possess high C IV EWs and low C IV blueshifts. Nevertheless, the derived scaling relations based on the reverberation-mapped sample are regularly applied to the quasar population with low C IV EWs and/or large C IV blueshifts, where any non-virial outflow-related contribution to the dynamics is significant. Much more complete coverage of the C IV-emission properties within the population of luminous quasars will come from the new SDSS-IV reverberation-mapping project (Shen et al. 2015) but, for now, additional direct comparison of C IV emission and low-ionization emission-line properties in the same quasars offers a way forward.

Near-infrared spectra, including the Hα emission line, for a sample of 19 quasars, at redshifts 2.0 < z < 2.7, have been obtained to complement existing SDSS optical spectra covering the C IV emission line. The 19 quasars were chosen to include a broad range of

C IV line blueshifts. Our aim is to directly test the reliability of C IV-based BH-mass estimates at high redshift for objects with a diverse range of C IV-line shapes. In particular, we will investigate potential systematic effects on the C IV-emission-based BH masses for quasars with large, $\gtrsim 1200$ km s^{-1}, C IV blueshifts, using the properties of the Hα emission line to provide BH-mass estimates for the objects unbiased by non-virial contributions to the emission-line profile. Examining higher redshifts, our work complements other studies which attempt to improve the reliability of BH-mass estimates which use the C IV line (e.g. Denney 2012; Runnoe et al. 2013b). However, the range of C IV blueshifts in our sample is significantly more extended, which will allow us to study systematic biases in C IV-based virial BH masses more directly, i.e. as a function of the C IV blueshift. Established relations to derive BH masses from emission-line properties are employed but an advantage of our approach is that C IV and Hα can be directly compared as a function of C IV emission-line shape. In Section 2, we describe how quasars were selected for rest-frame optical spectroscopy, before reviewing the C IV emission-line properties of high-luminosity quasars in the SDSS surveys in Section 3. The new near-infrared spectroscopic observations are outlined in Section 4. With spectroscopic coverage of the C IV and Hα emission lines available, the procedures used to quantify the line parameters are described in Section 5. The results of the spectral analysis in the context of BH masses and C IV blueshift are presented in Section 6, with a discussion of the significance of the systematic trends identified included in Section 7. The paper concludes with a summary of the main conclusions in Section 8. Throughout this paper, we adopt a Λ cold dark matter cosmology with $h_0 = 0.71$, $\Omega_M = 0.27$, and $\Omega_\Lambda = 0.73$. All wavelengths and equivalent width measurements are given in the quasar rest frame, and all emission-line wavelengths are given as measured in vacuum.

2 SAMPLE SELECTION

The parent sample for our investigation is the spectroscopic quasar catalogue of the SDSS (York et al. 2000) Seventh Data Release (DR7; Schneider et al. 2010). The SDSS DR7 catalogue contains moderate resolution ~ 3800–9180 Å spectra for 105 783 quasars. Shen et al. (2011) have compiled a catalogue of properties for the SDSS DR7 quasars including, at $z > 1.5$, measurements of the broad C IV $\lambda\lambda 1548.2$, 1550.8 emission line. Our aim is to explore the relationship between the Hα and C IV emission-line properties over the full dynamic range in C IV-emission shapes, with particular emphasis on quasars possessing large C IV blueshifts (see Section 3). The sample was restricted to objects with redshifts $2.14 < z < 2.51$ (7258 quasars), to ensure that the Hβ and Hα emission lines fall within the H and K bands, respectively, allowing us to observe both simultaneously with the appropriate grism configuration. Given the limited number of quasars for which near-infrared spectra could be obtained, the quasar sample was further restricted to objects that are radio-quiet (5980 quasars), show no evidence of broad absorption lines (BALs) in their spectra (5299 quasars), and are free from significant dust extinction. We removed radio-loud objects from our sample using the same radio-loud classification as Shen et al. (2011), and BAL quasars using the classifications of both Shen et al. (2011) and Allen et al. (2011). The removal of quasars with significant dust extinction was achieved by identifying quasars with $i - K$ colours redder than a parametric spectral energy distributions (SED) model + Small Magellanic Cloud-like extinction curve with $E(B - V) = 0.05$ (see Maddox et al. 2012). The K-magnitude was taken from the UKIRT Infrared Deep Sky Survey (UKIDSS; Lawrence et al. 2007) Large Area Survey (ULAS). The requirement to be in the ULAS footprint and have reliable K-band photometry reduced our sample of possible targets to 1683, and the $E(B - V)$ cut left 1204 in our sample. Finally, a flux-limit of $K < 18.5$ (AB) was applied to ensure that spectra of sufficient signal-to-noise ratio (S/N) could be obtained (412 quasars).

We were able to obtain new infrared spectra for 19 quasars from this sample of 412 possible targets (Section 4). The quasars included in this sub-sample were selected to have C IV-emission shapes which span the full range observed in the population. Reliably quantifying the distribution of C IV-emission shapes has been made possible thanks to redshift-determination algorithms (Hewett & Wild 2010, Allen & Hewett, in preparation) which are independent of the C IV-emission shape. Calculation of the C IV emission-line parameters is described in detail in the next section.

3 C IV BLUESHIFTS IN THE QUASAR POPULATION

Recognition that the C IV emission line in quasars can exhibit significant asymmetric structure, with an excess of flux to the blue of the predicted rest-frame transition wavelength, extends back to Gaskell (1982). Significant progress in understanding the relationship between changes in C IV-emission shape and quasar properties has come about through studies in which near-infrared spectra of the hydrogen Balmer lines have been obtained. Such studies typically involve samples of modest size and the location of the Balmer lines provides a reliable estimate of the quasar systemic redshifts; recent examples include Shen & Liu (2012) and Marziani et al. (2016). In Section 5, we adopt the same approach to estimate systemic redshifts for the quasar sample presented here with near-infrared spectra. However, improvements in the estimation of systemic redshifts from UV quasar spectra means that it is now possible to quantify the distribution of C IV blueshifts in the observed quasar population as a whole.

3.1 Quasar systemic redshifts

Historically, the parametrization of the C IV emission-line properties for quasars in large surveys has not proved straightforward because the C IV emission line has itself been used in the determination of the quasar redshifts. The SDSS provided the first catalogue of tens of thousands of redshift $z > 1.6$ quasars with spectra of adequate velocity resolution and S/N that effective statistical studies of the rest-frame UV emission-line properties, including line-shape, have proved possible.

The comprehensive compilation of quasar properties for the SDSS DR7 quasars by Shen et al. (2011) provides a natural starting point for population studies. In Fig. 1(a), we plot the C IV blueshift versus C IV-emission EW using the SDSS pipeline redshifts and the blueshifts calculated by Shen et al. (2011). The grey points show all SDSS DR7 quasars for which measurements exist and the orange circles show the 19 quasars with near-infrared spectra presented in this paper. A strong trend in the blueshift values as a function of line EW is not evident in Fig. 1; structure in the parameter space is being masked because the C IV emission line is itself being used in the determination of the quasar redshifts.

The redshift-determination scheme of Hewett & Wild (2010) provided much improved redshifts, not least because the redshift estimates for the majority of quasars were derived using emission-lines other than the C IV-line itself. Fig. 1(b) shows SDSS DR7 quasars in the same C IV parameter space as Fig. 1(a), but now using
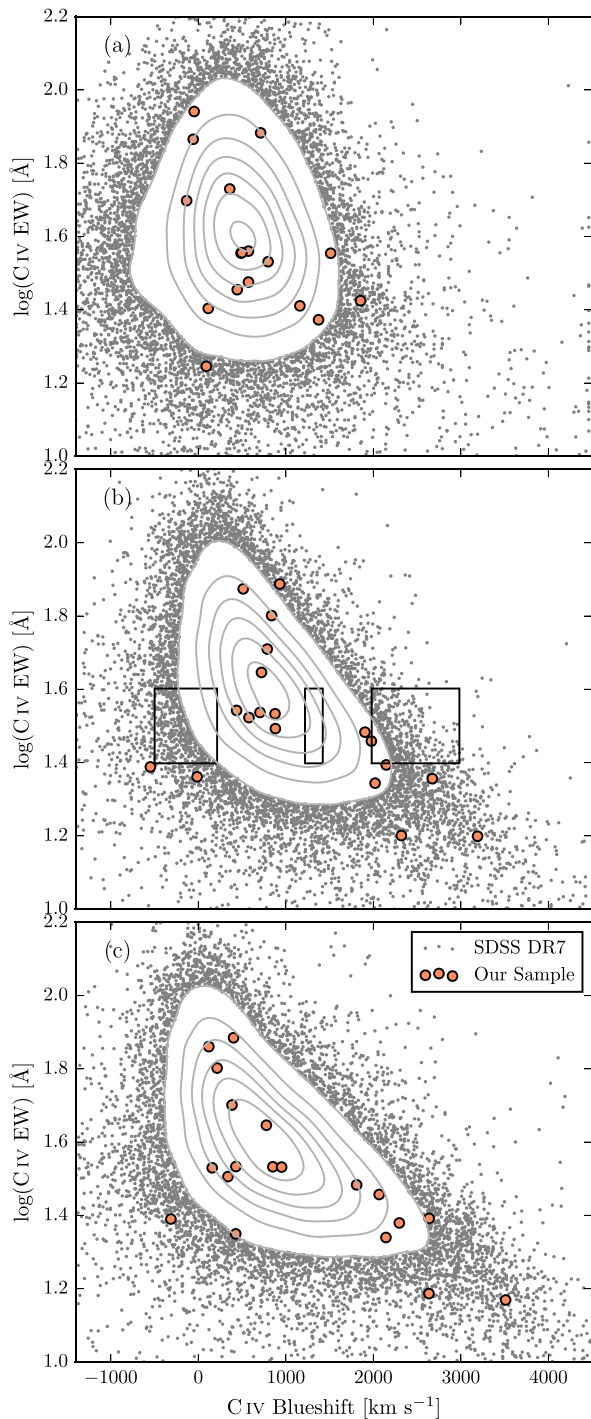
Figure 1. Rest-frame EW versus blueshift of the broad C IV emission line for 32 157 SDSS DR7 quasars at $1.6 < z < 3.0$ (grey) and our sample (orange). Panel (a) uses C IV line parameters from Shen et al. (2011) and SDSS pipeline systemic redshifts. Panels (b) and (c) use systemic redshifts from Hewett & Wild (2010) and Allen & Hewett (in preparation), respectively, and C IV line measurements described in Section 3.2. In regions of high point-density, contours show equally spaced lines of constant probability density generated using a Gaussian kernel-density estimator. The three rectangles in panel (b) show the regions of parameter space used to generate the composite spectra shown in Fig. 2.

Hewett & Wild (2010) redshifts. The improved redshift estimates are predominantly responsible for the differences seen in Figs 1(a) and (b); the appearance in Fig. 1(b) of the extension to high blueshift for quasars with low C IV EW is particularly evident.

The large systematic variation in the C IV emission-line profile within the population is evident from figs 11 and 12 of Richards et al. (2011). The plots and analysis in Richards et al. (2011) employ the quasar redshifts from Hewett & Wild (2010) but, as is evident from the figures, the systematic variation in the C IV shape is correlated with changes in the quasar SEDs, including the strengths of the [Si III] $\lambda1892$ and [C III] $\lambda1908$ emission lines in the rest-frame UV. As a consequence, the redshifts from Hewett & Wild (2010) still suffer from systematic errors that are correlated with the shape, and particularly the blueshift, of the C IV emission line. The nature of the systematic variations in the quasar UV SEDs are such that for quasars with close-to symmetric C IV profiles and line centroids close to the systemic redshift, the Hewett & Wild (2010) redshifts result in C IV blueshifts that are overestimated by a few hundred km s^{-1}, whereas, for quasars with strong blue-asymmetric C IV profiles and line centroids displaced significantly to the blue of the systemic redshift, the C IV blueshifts are underestimated by, in the most extreme cases, up to 1200 km s^{-1}.

Fig. 1(c) shows the C IV emission-line parameters calculated using a new redshift-estimation algorithm (Allen & Hewett, in preparation) that takes account of the quasar SED variations, producing redshifts independent of the large systematic shape changes seen in the C IV emission line. The low-ionization emission lines visible in the rest-frame UV (over wavelengths from Mg II $\lambda\lambda2796$, 2803 down to the O I $\lambda1304+$[Si II] $\lambda1307$ blend) using the new redshift-algorithm are located at rest-frame wavelengths in excellent agreement with the systemic redshift defined using the rest-frame narrow-line optical [O III] $\lambda\lambda4960$, 5008 and broad-line H β and Hα.

The systematic trends seen in Fig. 1(b), in particular the extension to high blueshift at low C IV EW, become more apparent in Fig. 1(c), as expected from consideration of the known SED-related errors in the redshifts from Hewett & Wild (2010). A population of quasars with only modest blueshifts and low EW is also apparently still present.

3.2 C IV emission-line blueshift measurements

The differences in the distribution of C IV emission-line properties seen in the three panels of Fig. 1 are due primarily to the change in the systemic redshift estimates. It is also necessary, however, to obtain a measure of the C IV emission-line 'location' in order to calculate the blueshifts. When working with moderately sized samples, parametric fits to the emission-line profile may be undertaken using careful mask-definition to minimize the effect of absorption features on the profiles used for the parametrization, and this is the approach we follow below in Section 5. Effective analysis of the tens of thousands of spectra from SDSS DR7, and now DR12, however, requires a more robust scheme to determine a C IV-blueshift estimate that is not very sensitive to the range of S/N among the spectra or the presence of narrow absorption systems within the C IV emission profile. Shen et al. (2011) provide a discussion (their section 3) of the factors that affect the measurement of broad emission lines in quasar spectra of modest S/N. Their careful analysis of the C IV emission properties employed the results of parametric fits of three Gaussians to the spectra. Our own experiments in quantifying the C IV emission properties of SDSS spectra showed that a simple non-parametric measure of the C IV emission location reduced the

number of outliers significantly. Visual inspection of spectra demonstrated that the improvement is due primarily to the identification of, and interpolation over, associated and outflow absorption systems, which forms part of the non-parametric measurement scheme.

We therefore chose to use a non-parametric scheme to measure the blueshift of the C IV line, which we will now describe. A continuum is first defined as a power law of wavelength, $f(\lambda) \propto \lambda^{-\alpha}$, with the slope, α, determined using the median[2] values of the flux in two continuum windows at 1445–1465 and 1700–1705 Å (the same wavelengths as adopted by Shen et al. 2011). The C IV emission line is taken to lie within the wavelength interval 1500–1600 Å, a recipe that is commonly adopted (e.g. Shen et al. 2011; Denney et al. 2013). To reduce the impact of narrow absorption systems on the emission-line profile, a 'pseudo continuum' is defined by applying a 41-pixel median filter to the quasar spectrum. Pixels within the C IV profile that lie more than 2σ below the pseudo-continuum are deemed to be affected by absorption and added to an 'absorber'-mask. Two pixels on either side of each such pixel are also included in the mask. For each masked pixel, the flux values in the spectrum are replaced by values from the pseudo-continuum.

The wavelength that bisects the cumulative total line flux, λ_{half}, is recorded and the blueshift (in km s^{-1}) defined as $c \times (1549.48 - \lambda_{\text{half}})/1549.48$, where c is the velocity of light and 1549.48 Å is the rest-frame wavelength for the C IV doublet.[3] Positive blueshift values indicate an excess of emitting material moving towards the observer and hence outflowing from the quasar. Hewett & Wild (2010) redshifts are used to define the quasar rest frame.

3.3 Sample selection – C IV properties

The primary aim of the paper is to investigate the potential systematic effects on the C IV-emission based BH masses for quasars with large, $\gtrsim 1200$ km s^{-1}, C IV blueshifts, using the properties of the Hα emission line to provide BH-mass estimates for the objects unbiased by non-virial contributions to the emission-line profile. The orange symbols in Fig. 1 show the C IV parameters of our quasar targets for which near-infrared spectra of adequate S/N were obtained. These quasars were selected using our non-parametric blueshift measures (based on the Hewett & Wild 2010 redshifts). The sample of 19 quasars spans the full dynamic range in C IV parameters based on the Hewett & Wild (2010) systemic redshifts and the coverage is in fact even more complete when using the forthcoming SED-independent redshifts from Allen & Hewett (in preparation). As is evident from the sparsity of quasars with large C IV blueshifts when the SDSS pipeline systemic redshifts are used (Fig. 1a), improvements in the estimation of systemic redshifts from UV spectra have been a crucial factor in allowing us to reliably select a sample of quasars with a range of C IV blueshifts. In subsequent sections, we re-derive the systemic redshifts and C IV blueshifts for this sample using parametric fits to the Hα and C IV emission (the former from our near-infrared observations). Thus, while the systematic trends in BH masses inferred from measurements of the C IV emission line depend on the distribution of C IV emission-line properties within the quasar population, the results of our analysis of the Hα and C IV

---

[2] The median is used to improve the robustness of the continuum estimate from the relatively small wavelength intervals.

[3] The adopted C IV rest-frame wavelength assumes an optically thick BLR, in which case the contribution from each component is equal. Adopting a 2:1 ratio (appropriate for an optically thin BLR) changes the blueshifts by ~ 80 km s^{-1}.
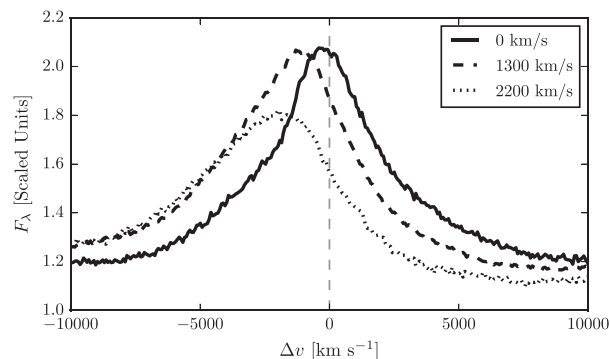

Figure 2. Composite spectra of the C IV emission line as a function of C IV blueshift for SDSS DR7 quasars. The quasars contributing to each composite are indicated in Fig. 1(b). Virtually, the entire C IV profile appears to shift blueward and the change in line shape is not simply an enhancement of flux in the blue wing of a still identifiable symmetric component. In order of increasing C IV blueshift, the composite spectra have FWHM 4870, 5610, and 6770 km s^{-1} and EW 33.1, 31.6, and 28.8 Å.

emission-line properties are independent of the redshifts used to produce the panels in Fig. 1.

3.4 Relation to virial BH-mass estimates

In general, researchers studying quasar demographics at high redshift adopt estimates of BH masses based on the width of C IV-emission, without reference to the blueshift of the C IV-emission (e.g. Vestergaard 2004; Kollmeier et al. 2006; Gavignaud et al. 2008; Vestergaard et al. 2008; Vestergaard & Osmer 2009; Kelly et al. 2010; Kelly & Shen 2013). The systemic redshift is often assumed to be given by the peak of the C IV emission, regardless of whether there is evidence that the line is shifted or not. Fig. 2 shows the shape of the C IV-emission in composite spectra constructed from SDSS DR7 quasars with EW(C IV) = 25–40 Å, as a function of C IV blueshift. Quasars classified as BALs, or possessing strong associated absorbers have been excluded, and the composite spectra shown are derived using an arithmetic mean of a minimum of 200 spectra at each blueshift. The blueshifts and EWs of the quasars contributing to each of the composites are indicated by the boxes in Fig. 1(b). The profiles show how, at large values of blueshift ($\gtrsim 2000$ km s^{-1}), the C IV-profile is displaced to the blue by amounts comparable to the FWHM of the profile.

A possible origin of the blueshifts is the presence of a disc wind (see Gallagher et al. 2015; Higginbottom & Proga 2015, for recent papers) but, irrespective of the physical origin of the high-blueshift C IV profiles, measures of the emission-line 'width' do not relate simply to virialized motions of the emitting gas under the gravitational influence of the BH. On the other hand, Denney et al. (2013) point out that any radiatively driven wind will have a velocity comparable to the escape velocity, i.e. approximately twice the virial velocity. Even if dominated by an outflow component, the C IV linewidth might therefore still be expected to relate to the BH mass.

4 OBSERVATIONS

Near-infrared spectra were obtained with the Long-slit Intermediate Resolution Infrared Spectrograph (LIRIS) mounted on the 4.2 m William Herschel Telescope (WHT) at the Observatorio del Roque de los Muchachos (La Palma, Spain). Observations took place over

four non-contiguous nights from 2015 March 31 to April 4. Approximately one night was lost due to poor weather and a further half-night was affected by poor transparency due to cloud. A 1 arcsec slit-width was employed and the LIRIS $H + K$ low-resolution grism was selected, which covers the spectral ranges 1.53–1.79 μm and 2.07–2.44 μm with a dispersion of 9.7 Å pixel^{-1}. The spatial scale of the instrument is 0.25 arcsec pixel^{-1}. Observations were divided into 60 s sub-exposures and performed in an ABBA nodding pattern, with the object placed at two positions along the slit 12 arcsec apart. Bright A0-5V stars were observed at similar airmasses to the targets in order to provide both telluric absorption corrections and a flux calibration of the quasar spectra.

The raw LIRIS data frames incorporate a known 'pixel shift' which was first removed from all frames using the LIRIS data reduction package LIRISDR. Subsequent data reduction was undertaken with standard IRAF[4] procedures. The flat-field images, which were taken at the beginning of each night via illumination of the dome, were averaged and normalized to remove any wavelength-dependent signature. Each individual two-dimensional spectrum was then flat-field corrected. Consecutive AB and BA pairs of two-dimensional spectra were subtracted to remove the sky background. All the subtracted AB/BA-pairs for a target were then averaged to give the final two-dimensional spectrum.

The size of the one-dimensional spectrum extraction windows, in the slit direction, varied from 6–10 pixels. To increase the S/N, optimal variance-weighted extraction with sigma clipping was employed. For the fainter objects in our sample, we were unable to trace the spectrum across the dispersion axis reliably and the trace from a telluric standard-star observation, observed at a similar airmass and time, was used instead. The wavelength calibration, using argon and xenon lamp exposures, resulted in root mean square errors in the range 1.01–1.71 Å, with a mean of 1.47 Å. The telluric standard star observations were reduced using the same steps described above. The stellar continuum was divided out of the standard-star spectrum, which was then divided into the quasar spectrum to remove telluric absorption features. The spectral type and magnitude of the standard star were used to flux calibrate the quasar spectrum both in a relative and absolute sense. Variable atmospheric conditions combined with the narrow slit width resulted in a significant level of uncertainty in the absolute flux calibration for the quasar observations. The use of the UKIDSS broad-band magnitudes (*H* and *K*) to normalize the spectra results in a significantly improved calibration.

Spectra with sufficient S/N for analysis of the Hα emission-line properties were obtained for a total of 19 quasars. Sixteen of the 19 quasars have been re-observed in the Sloan Digital Sky Survey-III: Baryon Oscillation Spectroscopic Survey (SDSS-III/BOSS; Dawson et al. 2013) and the spectra are available in the SDSS DR12 quasar catalogue (Pâris et al. 2016). As the BOSS spectra have higher S/N compared to those in DR7, we have used the BOSS spectra when available. A typical reduced LIRIS spectrum is shown in Fig. 3. A log of the observations, the quasar positions, magnitudes and redshifts, along with the S/N achieved for the Hβ, Hα and C IV emission-line regions (the last from the optical SDSS/BOSS spectra) are listed in Table 1. The S/N, which is given per resolution element, was measured in the continuum in the region around the
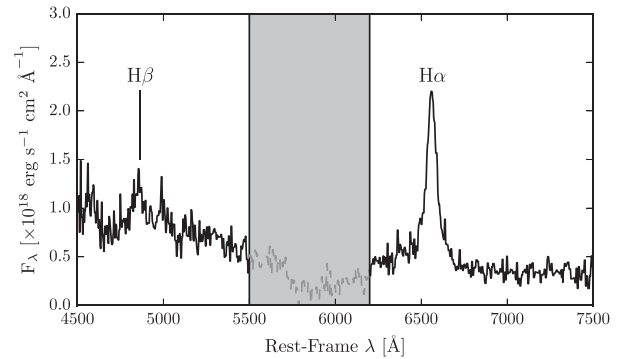
---

[4] IRAF is distributed by the National Optical Astronomy Observatory, which is operated by the Association of Universities for Research in Astronomy (AURA) under a cooperative agreement with the National Science Foundation.

Figure 3. LIRIS spectrum of SDSSJ1246+0426. The gap between the *H* and *K* bands (∼5500–6300 Å) has been greyed-out.

emission lines. The full SDSS name is given in Table 1; in the subsequent tables and text, we will refer to objects using an abbreviated name of the form SDSSJHHMM+DDMM.

Although the S/N is similar in the continuum regions adjacent to the Hα and Hβ emission lines, in practice, the much lower EW of Hβ compared to Hα meant that both parametric and non-parametric characterization of the emission-line parameters did not produce results that could be used in this investigation. The individual Hβ profiles were thus not employed, although a composite spectrum of the Hβ region is used below.

5 EMISSION-LINE MEASUREMENTS

Virial BH-mass estimators are calibrated using either the FWHM or dispersion (σ; derived from the second-moment velocity) of a broad emission line (e.g. Vestergaard & Peterson 2006; Park et al. 2013). Complications which are encountered when measuring linewidths include how to model the 'continuum' flux, where to define the limits of the line emission, and how to deal with absorption. All of these issues are exacerbated when working with low S/N data (see Denney et al. 2013, for a discussion). In Section 3.2, we measured the blueshift of C IV for tens of thousands of SDSS DR7 quasar spectra. This allowed us to quantify the distribution of C IV blueshift values and hence select a subset for near-infrared observations which have C IV blueshifts spanning the full range of this distribution (Fig. 1). A non-parametric scheme was employed because, in comparison to recipes involving the fitting of multiple Gaussian (or other parametric) profiles, it was found to be more robust and less sensitive to the range of S/N among the spectra and to the presence of narrow absorption systems within the C IV emission profile. In this section, we will use a different approach, and measure the line properties by fitting a parametric model to the data. When working with a small number of spectra, it is possible to use careful mask-definition to minimize the effect of absorption features on the profiles used for the parametrization. The purpose of the model fits is purely to best represent the intrinsic line profile, and no physical meaning is attached to the individual model components. We will now describe the parametric model and fitting procedure used for each emission line. The models were fit using a standard variance-weighted least squares minimization procedure employing the Levenberg–Marquardt algorithm. Prior to the fit, the spectra were visually inspected and regions significantly affected by absorption were masked and excluded.

Table 1. Summary of near-infrared spectroscopic observations with LIRIS.

SDSS name	SDSS DR	z^a	i_{SDSS}	UTC date	T_{exp} (s)	S/N(C IV)^b	S/N(H β)^b	S/N(Hα)^b
073813.19+271038.1	DR12	2.4508	18.80	2015-04-01	720	29.13	17.27	10.0
074352.61+245743.6	DR12	2.1659	19.09	2015-04-04	2160	8.64	18.68	11.43
080651.54+245526.3	DR12	2.1594	18.91	2015-04-01	1200	10.37	6.04	3.91
085437.59+031734.8	DR7	2.2504	18.41	2015-03-31	2520	26.58	5.82	3.09
085856.00+015219.4	DR12	2.1675	17.62	2015-04-04	1800	66.16	24.37	12.71
110454.73+095714.8	DR12	2.4238	19.12	2015-04-03	1440	19.41	10.75	7.81
123611.21+112921.6	DR12	2.1527	18.53	2015-04-04	1680	35.24	21.3	11.51
124602.04+042658.4	DR12	2.4473	18.49	2015-04-01	960	35.34	8.1	5.73
130618.60+151017.9	DR12	2.4020	19.00	2015-04-05	840	29.83	8.91	5.13
131749.78+080616.2	DR12	2.3791	19.04	2015-04-05	2880	19.25	5.6	3.32
132948.73+324124.4	DR12	2.1684	18.40	2015-04-01	2520	32.58	10.4	6.96
133646.87+144334.2	DR7	2.1422	18.84	2015-04-01	1200	15.2	23.82	16.34
133916.88+151507.6	DR12	2.3157	18.52	2015-04-03	2880	20.52	5.79	3.28
140047.45+120504.6	DR12	2.1722	18.29	2015-04-02	840	36.64	9.83	5.68
152529.17+292813.2	DR12	2.3605	17.52	2015-04-04	1440	80.55	2.17	1.5
153027.37+062330.8	DR12	2.2198	18.62	2015-04-04	1800	29.9	21.01	12.58
153848.64+023341.1	DR12	2.2419	17.56	2015-04-01	2520	64.82	5.63	3.56
161842.44+234131.7	DR7	2.2824	18.49	2015-04-04	1320	23.37	11.1	6.43
163456.15+301437.8	DR12	2.4901	18.29	2015-04-01	1920	36.06	9.44	8.63

Notes. ^{a}From Hewett & Wild (2010).
^{b}Measured in the continuum and quoted per resolution element.

Table 2. Summary of the fitting regions and the parameters of the models used to fit the C IV and Hα emission lines.

Name	Fitting region (km s^{-1}) C IV	Hα	Continuum region (Å) C IV	Hα	GH order C IV	Gaussians Hα	χ^2_ν C IV	Hα
0738+2710	−9570, 9770	−7530, 10 740	1445–1465, 1700–1705	6000–6250, 6800–7000	6	2	0.66	1.0
0743+2457	−9570, 9770	−7530, 10 740	1445–1465, 1700–1705	6004–6210, 6800–7000	2	2	0.84	1.0
0806+2455	−9570, 9770	−9219, 10 759	1445–1465, 1700–1705	6000–6250, 6800–7000	3	1	0.87	0.83
0854+0317	−9570, 9770	−7530, 10 740	1445–1465, 1700–1705	5989–6135, 6800–7000	3	2	0.91	0.85
0858+0152	−20 000, 7400	−7530, 10 740	1423–1428, 1700–1705	6000–6200, 6800–7000	2	2	0.94	0.96
1104+0957	−9570, 9770	−7530, 10 740	1445–1465, 1700–1705	6000–6250, 6801–6845	6	2	0.68	0.95
1236+1129	−15 363, 7650	−8904, 10 590	1445–1465, 1700–1705	6063–6210, 6800–7000	3	2	0.84	0.89
1246+0426	−9570, 9770	−7530, 10 740	1445–1465, 1700–1705	6000–6250, 6799–6906	4	2	0.66	0.83
1306+1510	−13 000, 7800	−7530, 10 740	1445–1465, 1700–1705	6000–6250, 6800–7000	2	3	0.73	0.18
1317+0806	−9198, 9755	−7530, 10 740	1445–1465, 1700–1705	6000–6250, 6800–7000	2	1	0.78	2.16
1329+3241	−12 000, 9000	−7605, 7406	1445–1461, 1700–1705	6000–6250, 6800–7000	3	2	0.61	0.84
1336+1443	−14 000, 10 000	−10131, 10 674	1445–1465, 1700–1705	6000–6250, 6800–7000	3	2	0.87	1.51
1339+1515	−12 000, 11 000	−7530, 10 740	1445–1465, 1700–1705	6046–6250, 6800–7000	4	1	0.69	0.14
1400+1205	−15 000, 10 000	−2000, 10 815	1445–1465, 1700–1705	6000–6250, 6800–7000	6	2	0.82	0.2
1525+2928	−9570, 9770	−7586, 8080	1459–1466, 1700–1705	6055–6251, 6800–7000	4	1	0.49	0.39
1530+0623	−12 000, 10 000	−7530, 10 740	1445–1465, 1700–1705	6127–6186, 6800–7000	4	3	0.84	1.14
1538+0233	−13 500, 9000	−7530, 10 740	1450–1465, 1700–1705	6000–6250, 6855–7002	4	2	0.61	0.82
1618+2341	−9190, 9770	−7530, 10 740	1445–1465, 1689–1697	6000–6250, 6800–7000	4	2	1.16	0.93
1634+3014	−9570, 9770	−8400, 8500	1445–1465, 1700–1705	6000–6250, 6736–6779	3	2	0.59	0.22

5.1 C IV

We first measure and subtract the local continuum emission, by fitting a power law to two windows on either side of the line emission, as described in Section 3.2. For a small number of objects, absorption features, or artefacts, in the spectrum-necessitated modest adjustments to the window extents, which are specified in Table 2. The continuum-subtracted spectra are then transformed from wavelength units into units of velocity relative to the rest-frame line-transition wavelength for the C IV doublet (1549.48 Å, assuming equal contributions from both components). The parametric model is ordinarily fit within the same 1500–1600 Å window used in Section 3.2, which corresponds to approximately ±10 000 km s^{-1} from the rest-frame transition wavelength. The line-window was extended if significant flux in the profile was present blueward of the

short wavelength limit. The adopted line-fitting windows, in units of velocity from the rest-frame transition wavelength, are given in Table 2.

To fit the C IV profile, we employed Gauss–Hermite (GH) polynomials, using the normalization of van der Marel & Franx (1993) and the functional forms of Cappellari et al. (2002). We allowed up to six components in the GH polynomial model, but in many cases, a lower order was sufficient; the polynomial order used for each line is given in Table 2. It is also a common practice to fit the C IV emission profile with two or three Gaussian components (e.g. Shen et al. 2011). We opted to use a GH-polynomial model primarily because it provided a significantly better fit to the most blueshifted and asymmetric C IV line (in SDSSJ0858+0152). Fig. 4 shows how a model with three Gaussian components underestimates the flux in the blue wing and overestimates the flux in the red wing of the line
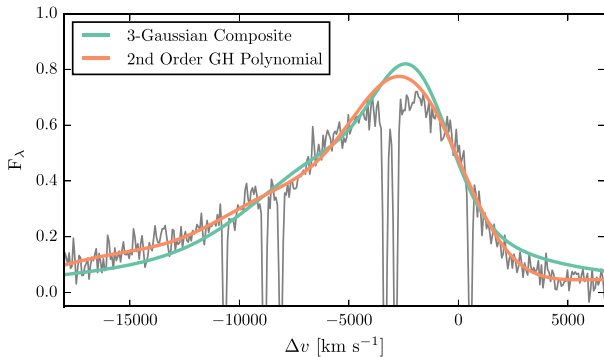
Figure 4. Second-order Gauss–Hermite (GH) polynomial and 3-component Gaussian fit to the C IV-emission line of SDSSJ0858+0152, which is the most blueshifted in our sample. We derive line parameters from the GH polynomial fit; using the Gaussian model changes the FWHM, line dispersion, and blueshift by -250, -150, and $500\,\mathrm{km\,s^{-1}}$, respectively. For the C IV lines of all other quasars in our sample, the GH polynomial and Gaussian models provide equally good fits.

profile. Using the Gaussian model rather than the GH polynomial changes the FWHM, line dispersion, and blueshift by -3, -3, and 10 per cent, respectively. We have highlighted SDSSJ0858+0152 because, of all the objects in our sample, the choice of model leads to the largest change in C IV line parameters. Even in this case, however, the differences are modest.

For every other C IV line in our sample, we found only marginal differences in our best-fitting line parameters when, rather than using a GH polynomial model, the C IV emission was fit using a composite model of up to three Gaussians. Our best-fitting parameters are also in good agreement with Shen et al. (2011), who employ a multiGaussian parametrization.[5] The scatter between the Shen et al. (2011) results and our own is 0.1 dex about the one-to-one relation and, as expected, is larger for lines with smaller EWs.

5.2 Hα

We employ the same continuum subtraction and fitting method as for C IV, with the continuum and fitting windows as given in Table 2. We adopt a rest-frame transition wavelength of 6564.89 Å to transform wavelengths into equivalent Doppler velocities. We used a simple model with up to three broad Gaussian components to fit the Hα emission line. We opted against parametrizing the Hα line using a GH polynomial because the extra degrees of freedom in this model did not improve the quality of the fits.[6] Upon inspection of the residuals from the fit, we also found no evidence that additional model components for narrow Hα, [N II]λλ6548, 6584 and [S II]λλ6717, 6731 were required. Furthermore, narrow [O III]λλ4960, 5008 emission is relatively weak in these spectra.

The sole exception is the Hα line in the spectrum of SDSSJ0738+2710. In addition to having the narrowest Hα line, this spectra also has the strongest narrow [O III] component (EW = 63 Å), which suggests that a contribution from the narrow-line region (NLR) might be important. Introducing a single Gaussian

---

[5] The Shen et al. (2011) parameters are derived from the SDSS DR7 spectra, whereas 16 out of 19 of our fits are to higher S/N BOSS DR12 spectra.

[6] The emission line parameters and subsequent analysis do not depend on whether line parameters from multiple-Gaussian or GH-polynomial model fits are used.

for the narrow emission, while retaining a double Gaussian for the broad emission, the FWHM of the broad component increases to $3400\,\mathrm{km\,s^{-1}}$ (compared to $1580\,\mathrm{km\,s^{-1}}$ without the narrow component). For consistency, the parameters quoted in Table 3 are from the model with no narrow component. However, because the properties derived from the emission-linewidth (the BH mass and the mass-normalized accretion rate) are strongly biased by the probable contribution from the NLR, SDSSJ0738+2710 is excluded from the analysis in Section 6.

5.3 Comparison of Hα and H β profiles

Virial BH-mass estimators are typically based on the width of H β. However, the Hα and H β emission is believed to originate from the same gas and the transformation between the emission-line velocity widths is expected to be well defined. Greene & Ho (2005), using a sample of 162 quasars with high S/N SDSS spectra, established the following relation between the Hα and H β FWHM:

$$\mathrm{FWHM(H\,\beta)} = (1.07 \pm 0.07) \times 10^3 \left(\frac{\mathrm{FWHM(H\,\alpha)}}{10^3 \mathrm{kms^{-1}}} \right)^{(1.03 \pm 0.03)}.$$ (1)

Greene & Ho (2005) found the root-mean-square scatter about this relation to be ~ 0.1 dex. We do not have a sufficient number of robust H β line measurements to test this relation directly. However, we are in the process of acquiring a much larger sample of quasars with near-infrared spectra covering Hα and H β at similar redshifts and luminosities to the sample presented here. The Hα and H β line widths of this sample are in excellent agreement with the Greene & Ho (2005) relation. To indirectly test the Hα/H β line-width relation for the sample presented here, we first constructed mean composite spectra in the Hα and H β emission-line regions to increase the S/N. The individual rest-frame spectra (defined using the wavelength of the Hα centroid) were interpolated on to a common wavelength grid. The spectra were then normalized using the continuum flux under the line centre, which was found by linearly interpolating between two emission-line free windows on either side of the line. Fig. 5 shows the composite Hα and H β line regions overlaid and, as expected, the line profiles are closely matched.

5.4 Emission-line parameters

In Fig. 6, we show our best-fitting models overlaid on the observed flux in the spectral regions around C IV and Hα. The spectra are presented in order of increasing C IV blueshift. The Doppler velocities have been shifted so that the Hα emission-line centroid is at $0\,\mathrm{km\,s^{-1}}$. The y-axes of the data-minus-model residual plots have deliberately been scaled by the spectrum flux errors. The model fits are generally very good with only minimal systematic residuals. The only significant features seen in the residual C IV spectra correspond to the location of narrow absorption lines which were excluded in the fitting procedure. The continuum windows for a number of the Hα lines extend close to the edges of the *K* band and uncertainties in the flux calibration, and hence continuum level, are almost certainly responsible for the low-amplitude, large-scale, systematic residuals seen in a number of objects (e.g. SDSSJ 0806+3455, 0858+0152, 1400+1205, 1538+0233). The amplitudes are, however, small and redefining the continuum levels to eliminate the residuals has only a very small effect on the line-profile parameters used in the analysis.

The systemic redshift (defined using the Hα peak), the C IV blueshift, the line FWHM, dispersion, and EW of Hα and C IV

Table 3. Summary of emission-line properties derived from parametric model fits to Hα and C IV.

| Name	z (Hα)	Blueshift (km s⁻¹) C IV	FWHM (km s⁻¹) C IV	FWHM (km s⁻¹) Hα	σ (km s⁻¹) C IV	σ (km s⁻¹) Hα	EW (Å) C IV	EW (Å) Hα
0738+2710	2.4396	50 ± 21	2255 ± 42	1503 ± 95	2916 ± 42	1789 ± 95	54 ± 2	532 ± 43
0743+2457	2.1662	692 ± 210	5924 ± 536	6036 ± 511	3801 ± 536	3904 ± 511	33 ± 4	351 ± 23
0806+2455	2.1542	389 ± 115	3435 ± 267	4059 ± 403	3387 ± 267	1724 ± 403	51 ± 4	488 ± 56
0854+0317	2.2475	-403 ± 134	3940 ± 354	4436 ± 522	3448 ± 354	3146 ± 522	24 ± 2	617 ± 90
0858+0152	2.1692	4354 ± 82	8412 ± 384	3155 ± 80	5298 ± 384	3758 ± 80	28 ± 1	622 ± 23
1104+0957	2.4217	-299 ± 55	3590 ± 112	3307 ± 334	3259 ± 112	2723 ± 334	70 ± 3	441 ± 72
1236+1129	2.1559	2828 ± 99	7540 ± 271	3152 ± 131	4168 ± 271	3277 ± 131	28 ± 1	631 ± 29
1246+0426	2.4393	325 ± 145	4126 ± 88	4268 ± 472	3901 ± 88	2543 ± 472	48 ± 1	536 ± 77
1306+1510	2.3989	2043 ± 84	6660 ± 158	2626 ± 330	3905 ± 158	2145 ± 330	36 ± 1	349 ± 52
1317+0806	2.3748	437 ± 289	5256 ± 182	7188 ± 946	3675 ± 182	3033 ± 946	33 ± 2	374 ± 67
1329+3241	2.1637	652 ± 113	4528 ± 491	4908 ± 410	3819 ± 491	3350 ± 410	35 ± 2	428 ± 35
1336+1443	2.1466	3668 ± 345	8780 ± 1003	2954 ± 67	3772 ± 1003	3227 ± 67	20 ± 2	523 ± 17
1339+1515	2.3207	133 ± 184	3865 ± 935	8816 ± 1072	4501 ± 935	3627 ± 1072	44 ± 2	500 ± 98
1400+1205	2.1672	2492 ± 107	7590 ± 290	3231 ± 227	4363 ± 290	3103 ± 227	25 ± 1	642 ± 55
1525+2928	2.3572	612 ± 536	5697 ± 128	6360 ± 1915	4303 ± 128	2696 ± 1915	41 ± 1	458 ± 186
1530+0623	2.2169	1471 ± 108	5397 ± 302	3073 ± 145	4092 ± 302	2664 ± 145	26 ± 1	499 ± 28
1538+0233	2.2420	2018 ± 80	5567 ± 100	2892 ± 253	3596 ± 100	2415 ± 253	25 ± 1	465 ± 75
1618+2341	2.2755	42 ± 53	2516 ± 161	2669 ± 175	3312 ± 161	2359 ± 175	34 ± 2	425 ± 39
1634+3014	2.5018	1509 ± 223	6835 ± 745	6210 ± 900	4566 ± 745	3236 ± 900	26 ± 1	327 ± 65
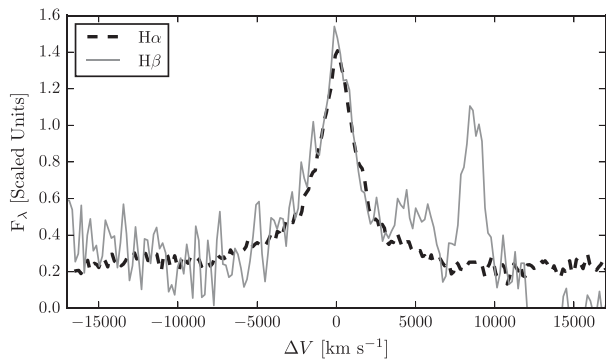
Figure 5. The Hα and H β emission-line regions in the median composite spectrum, shown as function of the velocity shift from the respective predicted line peak wavelengths. The line fluxes have been scaled in order for the profile shapes to be readily compared. The Hα and H β line profiles are very similar, which suggests a tight correlation between the Hα and H β linewidths. Quasar narrow-line emission from [O III] λ5008.2 is visible but, overall, the [O III] λλ4960, 5008 emission is relatively weak in these spectra.

are all given in Table 3. Both the FHWM and the dispersion (σ) have been corrected for instrumental broadening by subtracting the FWHM resolution (152 and 477 km s⁻¹ for SDSS/BOSS and LIRIS, respectively) in quadrature.[7]

Our definition of the C IV blueshift differs slightly in two ways from the values plotted for the quasar population in Fig. 1. First, we use the peak of our parametric model fit to the Hα line to define the quasar systemic-redshift.[8] Secondly, the centre of the C IV line is now defined as the wavelength that bisects the cumulative total flux of our best-fitting GH-polynomial model rather than of the data.

The monochromatic luminosity of the continuum at 1350 and 5100 Å, which are used to calculate virial BH-mass estimates, are

[7] For the dispersion, we first divide the FHWM resolution by 2.35, which assumes that the line profile is Gaussian.
[8] The Hα-derived redshifts are very closely in agreement with those from the forthcoming Allen & Hewett redshifts, which are plotted in Fig. 1(c).

given in Table 4. The luminosity at 1350 Å was taken from the spectral fits of Shen et al. (2011). The quasar rest-frame continuum at 5100 Å often lies at the edge, or beyond, the wavelength coverage of the LIRIS spectra. Monochromatic 5100 Å luminosities were therefore calculated from the fit of our parametric quasar model (described in Maddox et al. 2012) to the UKIDSS *H*- broad-band magnitude for each quasar. The model fits to the quasars are excellent, with residuals in SDSS and UKIDSS passbands under 10 per cent.

5.5 Emission-line parameter uncertainties

The 1σ error bars calculated from the covariance matrix in least-squares minimization will underestimate the true uncertainties on the line parameters, since they do not account for systematic errors such as the significant uncertainty introduced in the continuum subtraction procedure. To calculate more realistic uncertainties on our fitted variables, we employed a Monte Carlo approach. Artificial spectra were synthesized, with the flux at each wavelength drawn from a Normal distribution (mean equal to the measured flux and standard deviation equal to the known error). Our emission-line fitting recipe was then implemented on 5000 artificial spectra. Our parameter uncertainties are defined as the standard deviation of the best-fitting parameter values from these 5000 realizations. The uncertainty on the monochromatic continuum luminosity at 5100 Å was estimated via a very similar method – using the error on the UKIDSS *H*-band magnitude to run a number of realisations of our SED-fitting routine. The uncertainties on all derived quantities, such as the BH mass, are propagated through by assuming that the uncertainties are uncorrelated and independent.

Because of its sensitivity to the flux in the wings of the line profile, care must be taken to define an appropriate range over which to measure the line dispersion. This is particularly true of Lorentzian-like profiles with extended wings. In spectra of only moderate S/N, the line limits are difficult to determine unambiguously, which introduces an extra degree of uncertainty in line dispersion measurements. In common with previous work (e.g.

Vestergaard & Peterson 2006), by default, the dispersion was calculated within $\pm 10\,000$ km s^{-1} of the line centre, but this was extended when appropriate to avoid excluding a significant amount of line flux.

6 RESULTS

A fundamental assumption on which single-epoch virial BH-mass estimates are based is that the widths of the broad emission lines are directly related to the virial motions of the emitting clouds moving in the gravitational potential of the central BH. However, the C IV line profiles of the quasars in our sample with the largest C IV blueshifts indicate that non-virial motions, very likely due to outflows, are having a significant effect on the observed C IV emission velocity profile (e.g. Gaskell 1982; Baskin & Laor 2005; Sulentic et al. 2007; Richards et al. 2011; Wang et al. 2013). As shown in

Fig. 2, at fixed emission-line EW, virtually the entire C IV profile appears to shift blueward and the change in line shape is not simply an enhancement of flux in the blue wing of a still identifiable symmetric component. While gravity almost certainly plays a key role, determining the escape velocity for outflowing material, for example, it is clear that the virial assumption, on which single-epoch BH-mass measurements are predicated, is not straightforwardly applicable for the C IV emission line in quasars exhibiting large blueshifts.

The main aim of this paper is to investigate potential systematic trends in C IV-based single-epoch virial BH masses as a function of the C IV blueshift. Calibrations using H β (and therefore also Hα) are generally accepted to be the most reliable, since most reverberation-mapping employs the H β line and the *R–L* relation has been established using H β. Therefore, we will test the reliability of the C IV-based estimates by comparing C IV line profiles to Hα profiles in the same quasars.
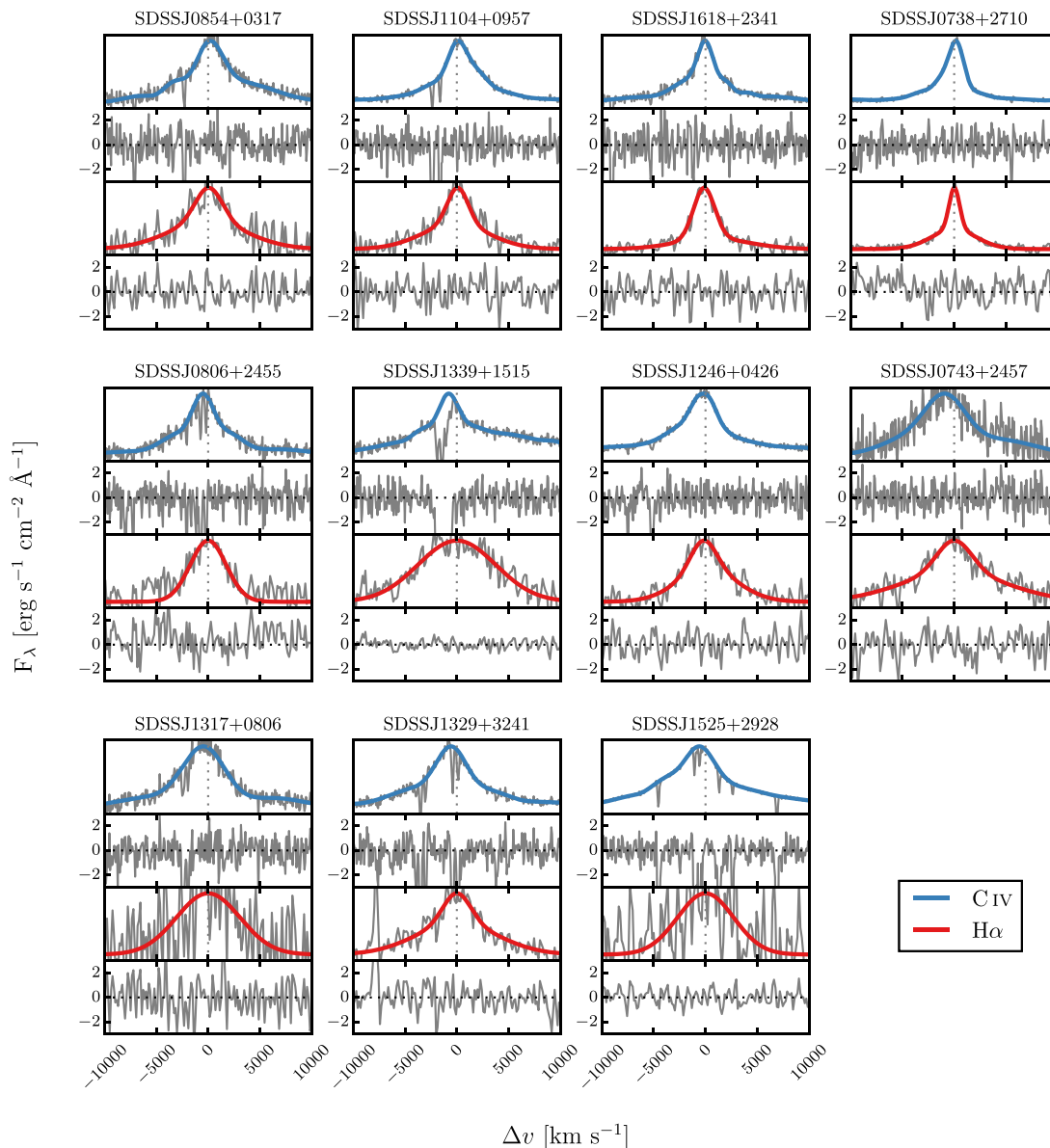

Figure 6. C IV (SDSS/BOSS) and Hα (LIRIS) emission lines and best-fitting model. Δv is the velocity shift from the line rest-frame transition wavelength, with the systemic redshift defined using the centroid of the fit to Hα. Objects are presented in order of increasing C IV blueshift relative to the Hα centroid. Below each fit, we plot the data-model residuals, scaled by the errors on the fluxes.
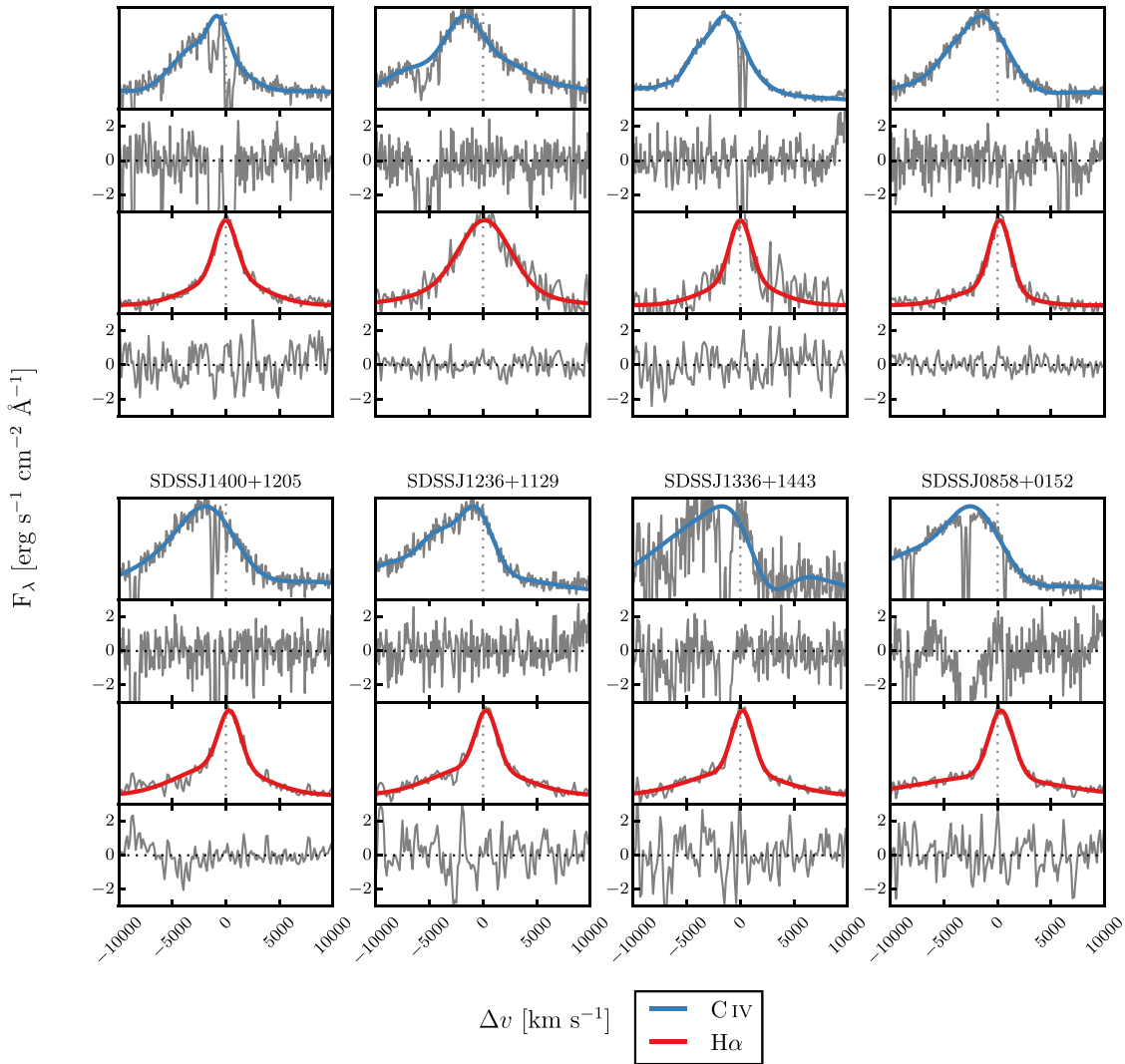
Figure 6 – *continued*

6.1 Characterising the emission-line profiles

There has been a considerable degree of attention paid to the effectiveness of different velocity-width measures of the C IV emission; specifically, the line FWHM and the dispersion, σ, derived from the second-moment velocity (e.g. Assef et al. 2011; Denney et al. 2013). The FWHM and line dispersion trace different parts of the broad-line velocity field, with the FWHM relatively more sensitive to any low-velocity core present and the line dispersion relatively more sensitive to the high-velocity wings. The shape of the line can be characterized by the ratio FWHM/σ. FWHM/$\sigma \simeq 2.35$ for a Gaussian profile, while FWHM/$\sigma \simeq 1$ for a peakier Lorentzian profile.[9] In practice, the line dispersion is almost certainly a more robust velocity indicator when the assumptions underlying the virial-origin of the emission-line velocity width are true and the spectral S/N and resolution are adequate. This was demonstrated by Denney et al. (2013) for a sample of quasars possessing a significantly smaller range in C IV blueshift than investigated here.

In reality, however, as highlighted by Denney (2012), contributions to the C IV emission-line profile from gas where virial motions do not dominate can be significant. Looking to the future, the results of the new reverberation-mapping projects (King et al. 2015; Shen et al. 2015) will show what fraction of the C IV emission line, as a function of velocity, does reverberate for quasars with an extended range of C IV emission shapes. The derivation of quantitative corrections to transform velocity-width measures from single-epoch to reverberation-only line profiles should then be possible.

As such information is not yet available, there is a strong rationale for investigating whether the systematic changes in the C IV emission-line profile can be used to improve the single-epoch BH-mass estimates derived using the C IV line. In the left-hand panels of Fig. 7, we show how the C IV FWHM, line dispersion, σ, and line shape, FWHM/σ, vary as a function of the blueshift. The C IV FWHM is correlated with the blueshift, with the median FWHM of quasars with the largest blueshifts a factor of 2 to 3 higher than quasars with only moderate blueshifts. The dispersion, however, does not show a similarly strong systematic variation.

Without knowledge of the C IV blueshifts, the dynamic range present in the FWHM and line dispersion measurements accords with the expectations from the study of Denney et al. (2013); the

---

[9] Strictly FWHM/$\sigma \rightarrow 0$ for a Lorentzian profile, but values close to unity are typical when the dispersion is calculated over a velocity range, $\simeq \pm 10\,000$ km s^{-1}, used to parametrize broad emission lines in quasar spectra.

Table 4. Monochromatic continuum luminosities used to derive bolometric luminosities and BH masses.

Name	log L_λ (erg s^{-1})	
	1350 Å	5100 Å
0738+2710	46.43 ± 0.02	46.14 ± 0.01
0743+2457	46.07 ± 0.02	45.93 ± 0.02
0806+2455	46.09 ± 0.01	45.95 ± 0.02
0854+0317	46.28 ± 0.01	46.27 ± 0.01
0858+0152	46.82 ± 0.00	46.37 ± 0.01
1104+0957	46.11 ± 0.03	45.92 ± 0.02
1236+1129	46.45 ± 0.01	46.01 ± 0.01
1246+0426	46.46 ± 0.01	46.13 ± 0.01
1306+1510	46.35 ± 0.01	46.00 ± 0.02
1317+0806	46.31 ± 0.01	46.02 ± 0.01
1329+3241	46.35 ± 0.01	46.08 ± 0.02
1336+1443	45.84 ± 0.02	45.95 ± 0.01
1339+1515	46.42 ± 0.01	45.97 ± 0.01
1400+1205	46.45 ± 0.01	46.05 ± 0.01
1525+2928	46.84 ± 0.01	46.50 ± 0.01
1530+0623	46.26 ± 0.01	45.97 ± 0.01
1538+0233	46.94 ± 0.00	46.51 ± 0.01
1618+2341	46.59 ± 0.01	46.10 ± 0.01
1634+3014	46.66 ± 0.01	46.16 ± 0.01

factor of $\simeq 4$ spread in the FWHM measurements indicating greater sensitivity to the emission-line profile shape than is the case for the dispersion, which varies by a factor of only $\simeq 2$. Adopting a value of $1200 \, \mathrm{km \, s^{-1}}$ to define 'low' and 'high' blueshift, the median C IV-emission dispersion for the low- and high-blueshift samples differ by only 10 per cent. It follows, therefore, that while the dispersion provides a relatively line-profile independent measure of the velocity width for quasars where the underlying assumption regarding the virial origin of the velocity width applies, quasars where the assumption is not true can be assigned apparently normal velocity widths and hence potentially incorrect BH masses.

To emphasize this point, in Fig. 8, we overlay the C IV line profiles of SDSSJ1236+1129 and SDSSJ1525+2928, whose dispersions (Table 3) are indistinguishable (4168 ± 271 and $4303 \pm 128 \, \mathrm{km \, s^{-1}}$, respectively). Notwithstanding the very similar dispersion values, the emission-line velocity fields differ dramatically and, therefore, the dispersion values cannot be measuring accurately the virial-induced velocity spread of the C IV emission in both quasars.

The analysis here, building on earlier work (including Sulentic et al. 2007; Shen & Liu 2012), confirms a link between C IV emission-line shape and blueshift, raising the prospect of developing a blueshift-dependent correction to single-epoch BH-mass estimates based on the C IV line. Expressed in another way, we are interested in testing if the significant systematic change in line shape as a function of C IV blueshift can be used to provide improved single-epoch BH masses from the C IV emission line. The tightness of the correlation we observe between the C IV FWHM and blueshift implies that such an approach may be more effective than using the C IV emission-line velocity dispersion without reference to blueshifts. A further practical advantage is that, given the typical S/N of current survey-quality spectra, virial BH-mass estimates for high-redshift quasars are usually based on the FWHM rather than the dispersion (e.g. Shen et al. 2011), which, being strongly affected by the continuum placement, is often found to be difficult to measure robustly (e.g. Mejia-Restrepo et al. 2016). As a first step towards the goal, below (Section 6.5), we investigate the apparent

systematic trends in the Hα FWHM and line shape as a function of C IV blueshift (shown in the right of Fig. 7).

6.2 Computing BH-mass estimates

Single-epoch virial BH-mass estimates normally take the form

$$M_{\mathrm{BH}} = 10^a \left(\frac{\Delta V}{1000 \, \mathrm{km \, s^{-1}}} \right)^b \left[\frac{L_\lambda}{10^{44} \mathrm{erg \, s^{-1}}} \right]^c , \qquad (2)$$

where ΔV is a measure of the linewidth (from either the FWHM or dispersion), L_λ is the monochromatic continuum luminosity at wavelength λ, and a, b, and c are coefficients, determined via calibration against a sample of AGN with reverberation-mapping BH-mass estimates. Several calibrations have been derived using different lines (e.g. H β, Mg II, C IV) and different measures of the linewidth (FWHM or dispersion) (FWHM or dispersion; e.g. McLure & Jarvis 2002; Vestergaard 2002; Vestergaard & Peterson 2006; McGill et al. 2008; Wang et al. 2009; Rafiee & Hall 2011; Park et al. 2013).

Reverberation-mapping measurements of nearby AGN have revealed the BLR to be stratified, with high-ionization lines, including C IV, emitted closer to the BH than low-ionization lines, including Hα and H β (e.g. Onken & Peterson 2002). Vestergaard & Peterson (2006) found that the C IV-emitting region is at approximately half the radius of the H β/Hα emitting region. Given the $\Delta V \propto R_{\mathrm{BLR}}^{-0.5}$ virial relation, this leads to the prediction that the C IV linewidths should be $\simeq 1.4$ times broader than Hα for a given BH mass. More recently, Denney (2012) found that there is a significant contribution from gas at larger radii to the C IV emission line, enhancing the profile at lower velocity and leading to smaller FWHM or dispersion values. The ratio of the line widths is therefore predicted to be lower than the factor of $\simeq 1.4$.

An alternate virial BH-mass calibration is proposed by Park et al. (2013), using an improved sample of AGN with reverberation-mapped masses. A major difference from the calibration of Vestergaard & Peterson (2006) is that Park et al. (2013), recognizing the poor correlation sometimes observed between the C IV and H β FHWM, allow the exponent on the velocity width (b in equation 2) to vary. Calibrating equation (2) against reverberation BH masses, they find a best-fitting value of $b = 0.56$, which is much less than the $b = 2.0$ in the strict virial regime. As a result, the derived BH masses are much less sensitive to the C IV emission-line properties. By contrast, our approach is to investigate whether a more complete parametrization of the C IV emission profile can be used to improve BH-mass estimates based on the conventional virial relation, with $b = 2.0$.

6.3 C IV-derived BH masses at low C IV blueshift

The Hα and C IV FWHM (dispersion) of the 10 quasars with C IV blueshifts $< 1200 \, \mathrm{km \, s^{-1}}$ are linearly correlated, as expected if the dynamics of the BLR clouds are dominated by virial motions. The median C IV/Hα FWHM (dispersion) ratio is 0.91 (1.22) with standard deviation 0.17 (0.28). Thus, the dispersion-based comparison results in a median C IV/Hα consistent with the value of $\simeq 1.4$ from assuming a virial origin for the emission but with a relatively large standard deviation. As predicted in Section 6.2, the FWHM-based comparison results in a systematically lower median C IV/Hα. However, the correlation between the C IV and Hα FWHMs is significantly tighter, lending support to the proposal that corrections to BH-mass estimates based on the C IV emission-line properties may be possible.
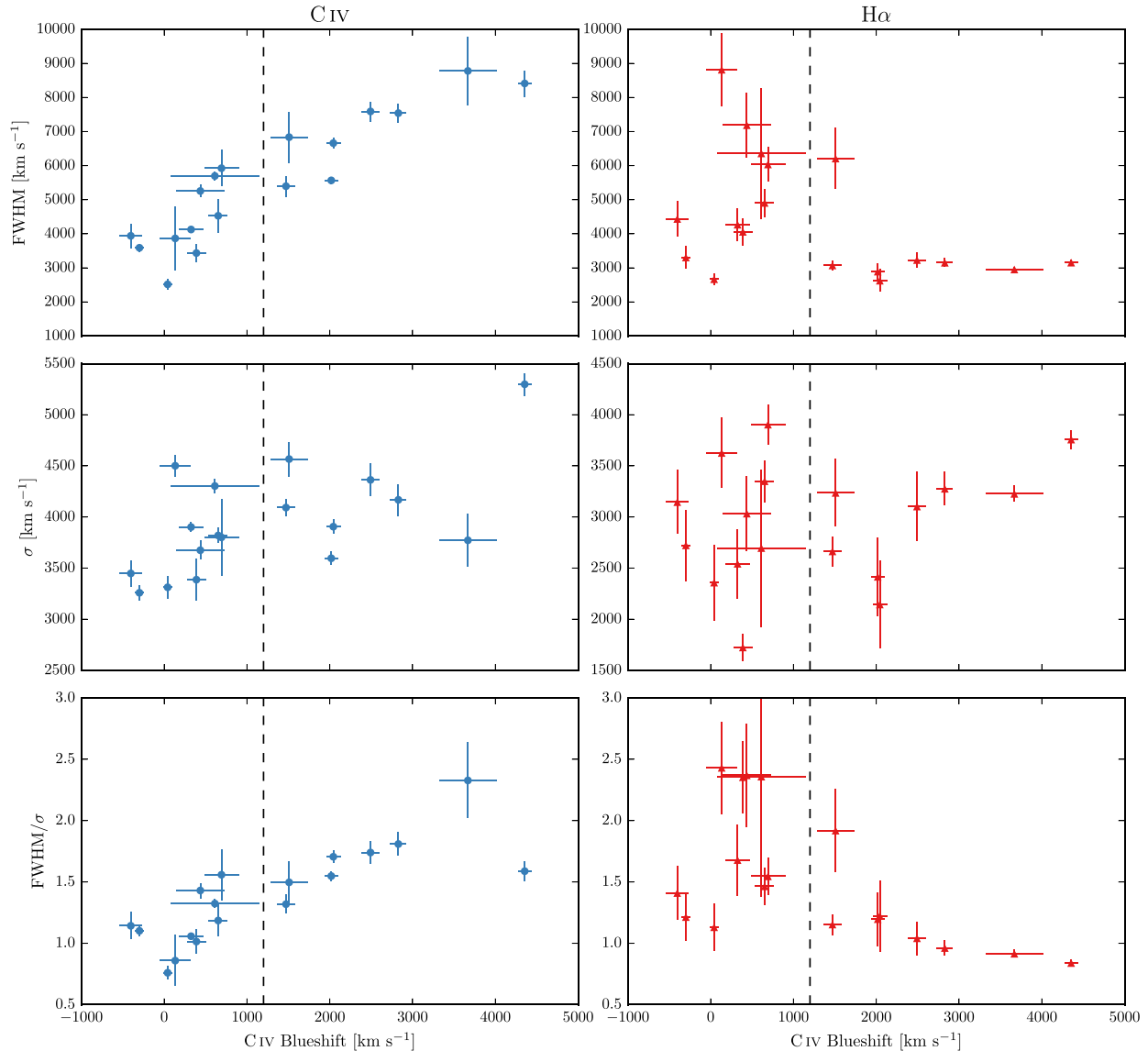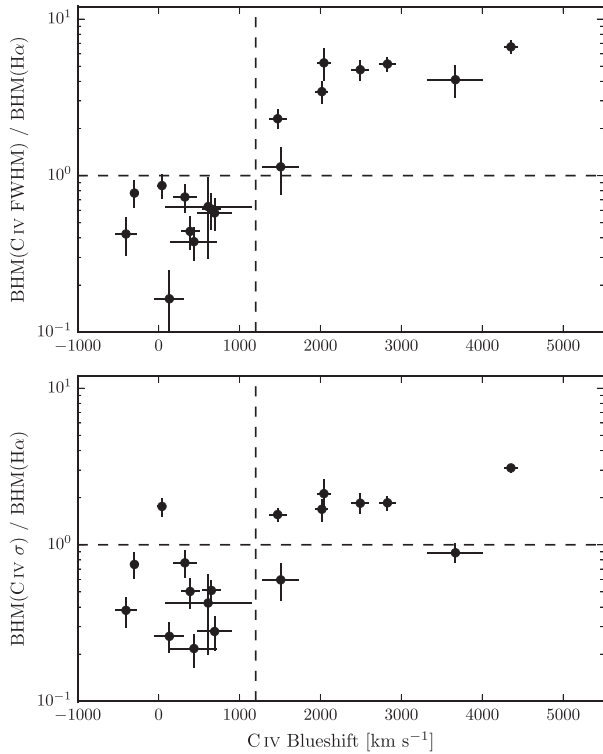
Figure 7. The FWHM, dispersion (σ) and shape (FWHM/σ) of C IV and Hα as a function of the C IV blueshift. The vertical line demarcates the 'high' and 'low' C IV blueshift regimes discussed in the text. At high blueshift, it is clear that BH masses estimated from the C IV FWHM (as is typically done at the redshifts considered) will be significantly larger than those estimated from the Hα FWHM.

Virial BH masses were calculated using the widely adopted Vestergaard & Peterson (2006) calibrations. The Vestergaard & Peterson (2006) C IV FWHM calibration uses the monochromatic continuum luminosity at 1350 Å to predict the BLR radius and corresponds to ($a = 6.66$, $b = 2$, $c = 0.53$) in equation (2). The calibration coefficient $a = 6.73$ in their equivalent dispersion-based relation. For the H β calibration, Vestergaard & Peterson (2006) use the monochromatic continuum luminosity at 5100 Å and calibration coefficients corresponding to ($a = 6.91$, $b = 2$, $c = 0.5$). BH masses are computed using the line and continuum properties given in Tables 3 and 4, and we convert our Hα emission-line velocity-width measures to predicted H β widths using equation (1).

As a direct consequence of the empirically small C IV/Hα FWHM ratio, the C IV-derived BH-mass estimates are systematically lower than the corresponding Hα-derived masses when the blueshift is small. This can be seen in Fig. 9, where for every quasar with a C IV blueshift <1200 km s^{-1} (i.e. to the left of the dashed line), the C IV-derived BH mass is smaller than the corresponding Hα-derived
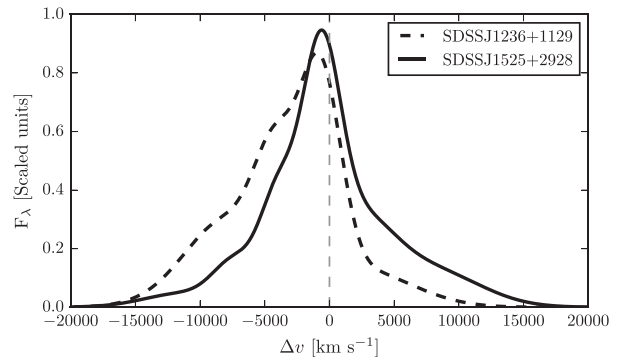
Figure 8. Comparison of the C IV line profiles of SDSSJ1236+1129 and SDSSJ1525+0426. Notwithstanding the essentially identical dispersion values, the emission-line velocity fields differ dramatically and, therefore, the dispersion values cannot be measuring accurately the virial-induced velocity spread of the C IV emission in both quasars.

Figure 9. Comparison of virial BH-mass estimates based on the C IV FWHM (top) and dispersion σ (bottom) and Hα FWHM as a function of the C IV blueshift. The horizontal line indicates agreement between C IV and Hα BH masses, and the vertical line demarcates the 'high' and 'low' C IV blueshift regimes discussed in the text. The BH masses of quasars with moderate C IV blueshifts are underestimated when using the C IV FWHM, while the masses of quasars with large blueshifts are severely overestimated. This situation cannot be corrected by changing the exponent on the FWHM (e.g. Rafiee & Hall 2011; Park et al. 2013) or the overall scaling in standard virial BH-mass relations.

mass. The median fractional difference between the two estimates is 0.60.

For the 10 quasars with low C IV blueshifts, we looked for correlations of the C IV/Hα FWHM ratio with other spectral properties. We found marginal evidence for an anticorrelation with the Hα FWHM (Spearman coefficient 0.58 with p-value 0.08). Among the quasars with Hα FWHM >4000 km s^{-1}, we found the mean C IV/Hα FWHM ratio to be 0.83, compared to 1.01 for the quasars with Hα FWHM <4000 km s^{-1}. Similar trends have been observed at low-z; in a sample of Boroson & Green (1992) quasars, Baskin & Laor (2005) found the C IV line to be broader than Hβ when the Hβ FWHM <4000 km s^{-1} and narrower when the Hβ FWHM >4000 km s^{-1}.

6.4 C IV-derived BH masses at high C IV blueshift

In Section 6.1, we have shown that the C IV emission at large C IV blueshift is not dominated by virial-induced motions due to the BH. The empirically derived increase in the C IV emission FWHM with blueshift leads directly to an overestimate of BH mass if the trend with blueshift is not taken into account. The availability of the Hα-spectra for the sample allows the quantification of the bias in inferred BH mass under the assumption that the Hα emission line provides a reliable BH mass.

Fig. 9 shows the ratio of the C IV- and Hα-FWHM derived BH masses as a function of the C IV blueshift. We see that for quasars with C IV blueshifts >2000 km s^{-1}, the C IV-based masses overestimate the Hα-based masses by as much as a factor of $\sim$5.

The existence of a trend in the C IV-dispersion values with C IV blueshift is evident from inspection of the bottom-left panel of Fig. 7 but the systematic trend relative to the spread at fixed blueshift is significantly smaller than when using C IV FWHM. Similarly, Fig. 9 shows, at most, only a weak increase in the ratio of C IV- and Hα-derived masses. Without knowledge of the C IV blueshifts, the distribution of C IV- and Hα-dispersion-based BH masses could be taken to be reassuring. Including the C IV-blueshift information, however, demonstrates that any such interpretation is inherently flawed because the origin of the C IV emission velocity width is not due to virial motions for a significant range of C IV blueshift. To reiterate the point made above (Section 6.1), we believe that using a greater knowledge of the line profile (i.e. both the FWHM and blueshift) is a better motivated (and more practical) approach to obtaining more reliable virial BH-mass estimates from the C IV line.

The number of objects in our sample is small but an important factor contributing to the significant correlation evident in the FWHM version of Fig. 9 is a change in the emission-line shape of Hα as the C IV blueshift increases. By comparing the distributions of the Hα FWHM and dispersion as a function of C IV blueshift (shown in the right-hand panels of Fig. 7), there is trend for the Hα lines to become peakier (with FWHM/σ approaching unity) as the C IV blueshift increases. Whether the size of the true systematic bias in BH masses inferred from C IV-emission FWHM is as large as shown in Fig. 9 will depend on the future parametrization of the reverberation component present in Hβ (and Hα) profiles for quasars with high luminosities and large C IV blueshifts.

In summary, Fig. 9 illustrates the extent to which key derived physical parameters, including the BH mass and $L/L_{\rm Edd}$, could be systematically in error when C IV-FWHM measures are used without incorporating the information from the C IV blueshifts. Other authors have proposed empirical corrections to C IV-based BH masses based on similar systematic trends seen in the C IV line shape (Denney 2012) and the continuum-subtracted peak flux ratio of the UV emission-line blend of Si IV+O IV (at 1400 Å) to that of C IV (Runnoe et al. 2013b). In Section 7.1, we apply these corrections to the quasars in our sample, and discuss the effect they have on the systematic bias seen in Fig. 9.

6.5 Population trends with C IV blueshift

Even with the caveat regarding the small sample size, the differences in the Hα emission profile as a function of C IV blueshift (Fig. 6) appear to be systematic. At C IV blueshift <1200 km s^{-1}, the Hα FWHM range is $\simeq$ 2700–8800 km s^{-1}, with mean $\simeq$5200 km s^{-1}. However, amongst the six quasars with C IV blueshift >2000 km s^{-1}, the mean Hα FWHM = 3000 km s^{-1}, with a scatter of just 200 km s^{-1}. The apparent trend of peakier Hα-emission, with FWHM/σ close to unity, at large C IV blueshift is enhanced by the modest increase in Hα EW with blueshift (Table 3). Amongst the low-C IV blueshift population, there are, in addition, quasars with broader and more Gaussian-like Hα line profiles, with FWHM/σ $\simeq$ 2.

The change in the Hα emission-line profiles as a function of C IV blueshift means that the Hα-FWHM derived BH masses at high blueshift are smaller than the sample mean. We transformed the observed luminosity into a mass-normalized accretion rate (Eddington
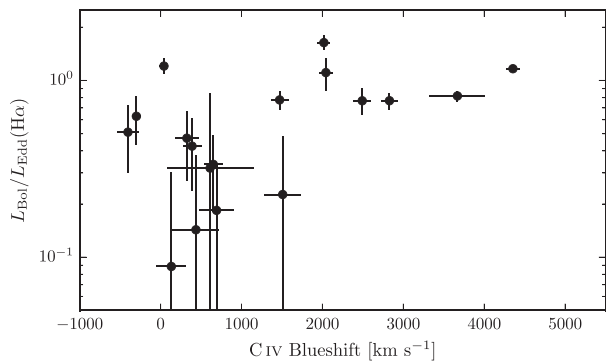
Figure 10. Hα-derived Eddington ratio versus C IV blueshift. At blueshift $\gtrsim 2000$ km s^{-1}, all quasars have high accretion rates ($L/L_{\mathrm{Edd}} \simeq 1$). This is in agreement with Kratzer & Richards (2015), but in contrast to what one would derive from naive use of C IV-based BH-mass scaling relations.

Figure 11. Comparison of BH-mass estimates derived from the FWHM of C IV and Hα as a function of the C IV blueshift (black circles), and after applying corrections to the C IV-derived mass based on the line shape (blue triangles; Denney 2012) and the peak flux ratio of the Si IV+O IV blend relative to C IV (red squares; Runnoe et al. 2013b). While the shape-based correction improves the consistency between BH-mass estimates in the low-blueshift population, only the Si IV+O IV/C IV peak flux-based correction is effective at high blueshifts (although a weak systematic remains).

ratio). To convert the monochromatic luminosity, which is observed into a bolometric luminosity, we use the bolometric correction factor given by Richards et al. (2006b) ($L_{\mathrm{bol}} = 9.26 L_{5100}$). Although there is evidence that the bolometric correction factor is a function of the luminosity, as well as of other parameters including the C IV blueshift (Krawczyk et al. 2013), the differences are small over the parameter range covered by our sample, and for simplicity, we adopt a constant factor.

The results, shown in Fig. 10, show that at large blueshifts quasars, are accreting at around their Eddington limits (Fig. 10). The converse is, however, not true, i.e. not all quasars with high Eddington ratios possess large C IV blueshifts (see Baskin & Laor 2005).

7 DISCUSSION

7.1 Biases in single-epoch C IV-based BH-mass estimates

The C IV line profiles of the quasars with the largest C IV blueshifts (in the bottom right of Fig. 1) demonstrate that non-virial motions are having a significant effect on the C IV BLR dynamics. At fixed emission-line EW, almost the entire C IV profile appears to shift blueward and the change in line shape is not simply an enhancement of flux in the blue wing of a symmetric component. It is clear that the virial assumption, on which single-epoch BH-mass measurements are predicated, is not straightforwardly applicable for the C IV-emission line in quasars exhibiting large blueshifts.

Quantitatively, the C IV-shape change is most apparent from the FWHM values, which are strongly correlated with the C IV blueshift. This trend has previously been identified, by comparison with Mg II at lower redshifts (Shen et al. 2008, 2011) and H β at higher redshifts (Shen & Liu 2012). We find that virial BH-mass estimates based on the C IV FWHM will overestimate the true mass by a factor of ∼5 for objects exhibiting the largest C IV blueshifts.

In contrast, the C IV line dispersion does not show a similarly strong dependence on the blueshift. This is a result of the shape of the C IV line profile being dependent on the blueshift; the low-blueshift profiles are peakier (FWHM/σ ≃ 1) than the high-blueshift profiles (FWHM/σ ≃ 2). Denney (2012) found that the level of contamination in single-epoch spectra from non-reverberating gas to be correlated with the shape (FWHM/σ) of the C IV profile. Their investigation was based on a sample of reverberation-mapped quasars, which have a narrow range of C IV emission-line shapes, including the absence of any objects with large C IV blueshifts. The FWHM/σ-
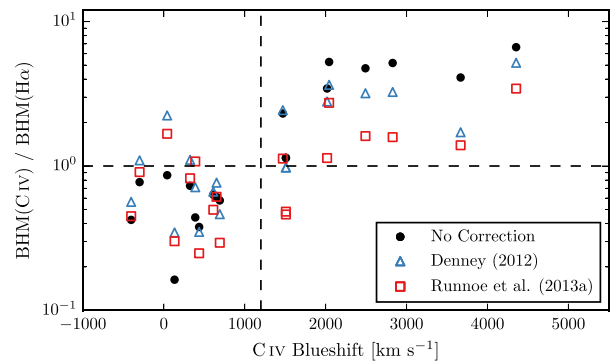
based correction to the C IV FWHM proposed by Denney (2012) increases the inferred BH masses by ∼0.2 dex at the low end of our C IV blueshift distribution, thereby reducing part of the systematic trend in the BH mass (Fig. 11). However, it is not applicable at the high C IV blueshift end, where velocity widths are likely dominated by non-virial motions. Based on the typical line shape of C IV in these high-blueshift quasars (FWHM/σ ≃ 2), the Denney (2012) correction decreases the predicted BH masses by ∼0.3 dex, which has only a moderate decreasing effect on the strong systematic (Fig. 11).

While the C IV-line dispersion is largely independent of the blueshift, it does not follow that dispersion-based BH-mass estimates are correct, because the underlying assumption regarding the virial origin of the C IV emission profile breaks down at large blueshifts. Furthermore, given the difficulty in obtaining reliable dispersion measurements from survey-quality spectra with limited S/N (e.g. Mejia-Restrepo et al. 2016), virial BH-mass estimates for existing large samples of high-redshift quasars are usually based on the FWHM (e.g. Shen et al. 2011). Our work therefore suggests that a viable recipe for obtaining more reliable BH-mass estimates for large numbers of quasars at high redshift is to measure both the FWHM and the blueshift, which together can be used to derive an FWHM corrected for the non-virial contribution.

Although we do not have enough quasars in our sample to derive a reliable quantitative correction to BH masses as a function of C IV blueshift, we are assembling a large sample of quasar spectra with coverage of both C IV and H β/Hα in order to empirically validate such a correction. Both Runnoe et al. (2013b) and Shen & Liu (2012) considered a similar approach, but concluded that a low-ionization broad line (e.g. Mg II), or features from the quasar NLR, are required to determine the systemic redshift and hence the C IV blueshift. Empirical tests of the reliability of the improved Hewett & Wild (2010) redshifts for the SDSS DR7 quasars (Shen 2016) and the availability of the largely SED-independent principal component analysis redshifts for DR10 and DR12 (Pâris et al. 2014, 2016) already allow meaningful corrections to BH-mass estimates for quasars exhibiting large C IV blueshifts. Our intention is, however, to determine a definitive correction formula using the redshifts from Allen & Hewett (in preparation) for both DR7 and DR12.

Given the difficulty of measuring reliable C IV blueshifts, Runnoe et al. (2013b) opted instead to use the continuum-subtracted peak flux ratio of the UV emission-line blend of Si IV+O IV (at 1400 Å) to that of C IV to correct for non-virial contributions to the C IV velocity width. This parameter was chosen because it showed the strongest correlation with the FWHM C IV/H β residuals, as well as with the strengths of optical [O III] and Fe II. The strengths of optical [O III] and Fe II, being parameters in EV1, are also correlated with the C IV blueshift (Sulentic et al. 2007). As the C IV blueshift increases, the EW decreases systematically (Fig. 1). The Si IV+O IV emission-line blend, however, shows significantly less systematic variation. Therefore, while the Runnoe et al. (2013b) Si IV+O IV-based correction is effective in practice, the C IV blueshift measurement provides a more direct measure of the non-virial contributions to the C IV velocity width.

In our sample, we find the 1400 Å/C IV peak flux ratio to be strongly correlated to the C IV blueshift (the Spearman coefficient for the correlation is 0.82, *p*-value 2E-5). As such, the correction to C IV-based virial masses proposed by Runnoe et al. (2013b, their equation 3) removes a large part of the systematic in the Hα/C IV FWHM residuals with the C IV blueshift (Fig. 11); the median C IV/Hα FWHM ratio at large C IV blueshifts (>1200 km s^{-1}) is reduced from 4.5 to 1.5. However, at low (<1200 km s^{-1}) C IV blueshifts, the trend for C IV to predict lower BH masses persists, and the scatter between the C IV- and Hα-based masses increases by a factor of 2. In accordance with our expectations, we find the FWHM C IV/Hα residuals to be more tightly correlated to the C IV blueshift (Spearman coefficient 0.82, *p*-value 3E-5) than to the 1400 Å/C IV peak flux ratio (Spearman coefficient 0.72, *p*-value 7E-4).

7.2 Possible systematic trends in Hα BH-mass estimates

In Section 6.5, we found that the quasars with large C IV blueshifts have systematically narrower Hα FWHM (Fig. 7). Using the standard virial BH-mass calibrations, this implies that the high C IV blueshift population have high accretion rates ($L/L_{Edd} \simeq 1$; Fig. 10). This interpretation requires some caution since the emission-line shape (characterized by the value of FWHM/σ) of Hα is also changing as a function of the C IV blueshift (Fig. 7). At low C IV blueshifts, there are a range of shapes, but all of the quasars exhibiting large C IV blueshifts have peaky Hα profiles with FWHM/$\sigma \simeq 1$. This raises the question of whether the Hα FWHM is a reliable proxy for the virial-induced velocity dispersion for the full range of Hα line shapes we have in our sample.

When calibrating the virial product to masses derived independently using the BH mass – stellar velocity dispersion ($M_{\odot}–\sigma$) relation, Collin et al. (2006) find that the scaling factor, *f*, is a factor of $\sim$2 larger for their Population '1' sources (with FWHM/$\sigma < 2.35$ and essentially equivalent to population A of Sulentic and co-workers and to the high-blueshift quasars here) than for their Population 2 (with FWHM/$\sigma > 2.35$). For single-epoch BH-mass estimates, assuming a constant value of *f*, as is normally done (e.g. Vestergaard & Peterson 2006), means that Population 1 masses will be underestimated and Population 2 will be overestimated. In the context of this result from Collin et al. (2006), our high-blueshift objects all possess peaky Hα-lines and, while our quasar sample probes much higher luminosities and masses, the true BH masses may also be underestimated. Adopting such an interpretation, the amplitude of the trend seen in Fig. 9 might not be so pronounced.

As mentioned in Section 1 and discussed in Richards et al. (2011), quasars with current reverberation-mapping measurements have a restricted range of C IV-line shapes. There are currently

very few reverberation-mapping measurements of quasars with large C IV blueshifts but the results of the large ongoing statistical reverberation-mapping projects (e.g. Shen et al. 2015) for luminous quasars at high redshift will go some way to establishing whether the quasar BLRs producing Balmer emission look the same for objects with very different C IV-emission blueshifts.

Although the EV1-trends (Sulentic et al. 2000b; Shen & Ho 2014) are most likely driven by the accretion rate, orientation may also have a role to play in determining the observed properties of the BLR. Shen & Ho (2014) argue that a large part of the scatter observed in the H β FWHM relates not to a spread in BH masses, but rather to the orientation of the BLR relative to the line of sight. For this to be true, the BLR would need to be in a flattened disc-like geometry, in which case the observed linewidth would increase with the inclination of the disc relative to the line of sight. Brotherton, Singh & Runnoe (2015) found that the core-dominance of radio-loud quasars, which is believed to be a reliable proxy for orientation, at least in a statistical sense, is significantly correlated with the H β FWHM and hence with the BH-mass estimates. This raises the question of whether the narrow Hα emission lines observed in the quasars with the largest C IV blueshifts could be an orientation effect. However, there is no evidence that the C IV blueshift is dependent on the orientation (inferred from the radio core-dominance; Richards et al. 2011; Runnoe et al. 2014). Furthermore, Leighly (2004) showed that the He II λ1640 emission-line properties of quasars with large C IV blueshifts are more consistent with differences in the SED rather than differences in the orientation. Collin et al. (2006) showed that orientation effects were also sub-dominant to the Eddington ratio in determining the shape of the H β line and the Hα line shape trend we observe is consistent with the finding of Marziani et al. (2003) that the H β emission profiles of high/low Eddington ratio low-*z* quasars and type 1 Seyfert nuclei are well fit by Lorentzian and double Gaussian profiles, respectively. Overall, therefore orientation does not appear to be the dominant effect in determining the C IV blueshift and correlated changes in the Hα line profile.

7.3 Accretion-rate trends in the quasar population

The blueshifting of C IV is usually interpreted as evidence for strong outflows resulting from the presence of a radiation-driven accretion-disc wind. Richards et al. (2002) found that quasars with large C IV blueshifts have weak He II. This is evidence for weak soft X-ray continuum emission (Leighly 2004), which would allow a strong line-driven wind to form. The strength of such a wind is predicted to be related to the quasar far-UV SED, which, in turn, could be related to the mass-accretion rate. This picture is therefore consistent with our finding that the quasars with large C IV blueshifts have high accretion rates.

All of the objects in our sample which exhibit large C IV blueshifts would be classified as population A in the Sulentic et al. (2000a) scheme based on the Hα FWHM (see Section 1). Our results therefore support the idea of the Sulentic et al. (2000a) A/B division being driven by the Eddington ratio, with population A sources possessing higher accretion rates. However, we also observe a number of quasars which have high Eddington ratios but do not have line profiles suggestive of strong outflows in the C IV BLR. This suggests that a high accretion rate is a necessary but not sufficient condition for the existence of outflows (Baskin & Laor 2005).

The two-dimensional nature of the C IV emission-line parametrization and the apparent anticorrelation between C IV EW and C IV blueshift suggests that the quasar population exhibits a continuum of properties. As such, more accurate C IV blueshift

measurements for SDSS quasars should allow an improved mapping between the C IV-emission properties and key physical parameters of the quasars. This includes improving our understanding of the origin of quasars with exceptionally weak, blueshifted C IV emission (weak emission-line quasars; Luo et al. 2015) which could be exotic versions of wind-dominated quasars (Plotkin et al. 2015).

7.4 The BAL parent population

Classical high-ionization BAL (HiBAL) quasars are also predominantly population A objects in the scheme of Sulentic et al. (2000a). There are no HiBAL quasars in our sample by design (Section 2) but it is generally accepted that quasars which show high-ionization BALs are likely to be radiating with relatively high L/L_{Edd} (e.g. Zhang et al. 2014). We therefore propose that the subset of the quasar population that exhibits large C IV-emission blueshifts, with high-EW and narrow-Hα emission lines, may be directly related to the HiBAL quasar population – perhaps even the 'parent' population (Richards 2006). A prediction of such a linkage is that near-infrared observations of the rest-frame optical spectra of HiBAL quasars will show strong, relatively narrow, Balmer emission lines, very similar to those of the quasars with high C IV blueshifts presented in this paper (see Runnoe et al. 2013a, for such a study).

7.5 The frequency of quasars with high accretion rates

Quantifying the frequency of quasars producing outflows as a function of key parameters, e.g. quasar luminosity, BH mass, redshift,...will be important to constrain models of quasar-galaxy evolution. At fixed BH mass, the intrinsic and the observed fraction of quasars exhibiting properties that depend on the Eddington ratio can differ significantly. As an illustration, we consider the implications for the intrinsic fraction of quasars possessing large C IV blueshifts given the observed numbers in the $m_i < 19.1$ flux-limited subsample of the SDSS DR7 quasar catalogue, from which our quasar sample is effectively drawn (Section 2). In order to estimate the size of the selection effect, we considered the detection probability for a much-simplified quasar population. We assume that all quasars with C IV blueshifts $>1200\,km\,s^{-1}$ have enhanced accretion rates relative to the 'normal' population (with C IV blueshifts $<1200\,km\,s^{-1}$). If the accretion rate of the high-blueshift population is double the rate of the low-blueshift population (which is true in an average sense – see Fig. 10), then the high-blueshift population will be brighter by $\simeq 0.75$ mag. Under the assumption that the BH-mass distribution is independent of the C IV blueshift, the high-blueshift population will then be overrepresented in a flux-limited sample. To estimate the size of the bias, we need to know how many more quasars, at redshifts $2 < z < 2.5$, there are with $m_i < 19.1 + 0.75 = 19.85$ relative to $m_i < 19.1$. This is the fraction of the population which, as a consequence of having enhanced accretion rates, are boosted above the survey flux limit. The main colour-selected SDSS DR7 quasar catalogue extends only to $m_i = 19.1$ and, assuming the luminosity function is continuous,[10] we thus use the number counts at $m_i < 19.1$ and $m_i < 18.35$, which differ by a factor of $\simeq 4$.

At redshifts $2 < z < 2.5$, there are 3834 quasars with C IV blueshifts $<1200\,km\,s^{-1}$ and 2484 with blueshifts $>1200\,km\,s^{-1}$ in the SDSS DR7 $m_i < 19.1$ quasar sample, a ratio of ~2:1. The above calculation, although much idealized, suggests that the intrinsic

fraction of high-blueshift quasars is a factor of 4 smaller than in the flux-limited sample (i.e. ~15 per cent of the UV-selected non-BAL quasar population).

8 CONCLUSIONS

We have presented an analysis of biases in C IV-derived virial BH masses of high-luminosity ($L_{bol} \sim 47$ erg s^{-1}) quasars at redshifts ~2.5 from the SDSS. Many authors have reported a large scatter between C IV- and Hα/Hβ-based masses, and part of this scatter has been shown to correlate with the C IV blueshift (Shen & Liu 2012). The blueshifting of C IV is usually interpreted as evidence for strong outflows which, most likely, result from the presence of a radiation line-driven accretion-disc wind. Our study is the first to examine this bias systematically across the full range of C IV emission-line blueshifts observed in the SDSS sample. In particular, we have used rest-frame optical spectra of 19 quasars in the redshift range $2 < z < 2.7$ to directly compare C IV and Hα emission properties as a function of the C IV blueshift. We reach the following conclusions.

(i) A strong correlation between C IV velocity width and blueshift is found and at large blueshifts, $>2000\,km\,s^{-1}$, the velocity widths are dominated by non-virial motions. This suggests that the assumption that velocity widths arise from virial-induced motions, on which single-epoch BH-mass measurements are predicated, is not straightforwardly applicable to these high-blueshift quasars.

(ii) We use the Hα emission line to provide BH-mass estimates that are unbiased by non-virial contributions to the velocity width. We find that the C IV-based BH masses of quasars with low C IV blueshifts are systematically underestimated (by a factor of ~1.7), whereas the masses of quasars with large blueshifts are severely overestimated (by a factor of ~5).

(iii) We find a systematic change in the shape of the Hα line profile as a function of the C IV blueshift. Specifically, the Hα line profiles of the quasars with high C IV blueshifts are all 'peaky' with FWHM/σ close to unity.

(iv) We suggest that the high C IV blueshift quasars are high Eddington ratio objects that are inherently rare (comprising ~15 per cent of the UV-selected sample), but are being boosted in number by a factor of ~4 in the flux-limited SDSS sample.

With a relatively small sample of 19 quasars, we have been able to uncover systematic trends in the C IV and Hα emission-line shapes as a function of the C IV blueshift. This confirms the prospect of developing a blueshift-dependent correction to C IV-based single-epoch BH-mass estimates using a larger samples of luminous quasars with both rest-frame UV and rest-frame optical spectroscopy. We are currently in the process of assembling such a sample, which will contain ~300 luminous quasars, 80 per cent at redshifts $z \geq$ 2. A new SED-independent redshift-estimation algorithm (Allen & Hewett, in preparation) makes it possible to quantify the distribution of C IV blueshifts in the observed quasar population as a whole, thereby allowing us to make empirical corrections to C IV-based BH masses for all luminous, high-redshift SDSS/BOSS quasars.

---

[10] The luminosity function and number counts vary only smoothly (e.g. Ross et al. 2013) for the magnitude and redshift range used here.

REFERENCES

Allen J. T., Hewett P. C., Maddox N., Richards G. T., Belokurov V., 2011, MNRAS, 410, 860

Assef R. J. et al., 2011, ApJ, 742, 93

Baskin A., Laor A., 2005, MNRAS, 356, 1029

Bentz M. C. et al., 2009, ApJ, 705, 199

Boroson T. A., Green R. F., 1992, ApJS, 80, 109

Boyle B. J., Terlevich R. J., 1998, MNRAS, 293, L49

Brandt W. N., Hasinger G., 2005, ARA&A, 43, 827

Brotherton M. S., Singh V., Runnoe J., 2015, MNRAS, 454, 3864

Brotherton M. S., Runnoe J. C., Shang Z., DiPompeo M. A., 2015, MNRAS, 451, 1290

Cappellari M., Verolme E. K., van der Marel R. P., Verdoes Kleijn G. A., Illingworth G. D., Franx M., Carollo C. M., de Zeeuw P. T., 2002, ApJ, 578, 787

Collin S., Kawaguchi T., Peterson B. M., Vestergaard M., 2006, A&A, 456, 75

Dawson K. S. et al., 2013, AJ, 145, 10

Denney K. D., 2012, ApJ, 759, 44

Denney K. D. et al., 2010, ApJ, 721, 715

Denney K. D., Pogge R. W., Assef R. J., Kochanek C. S., Peterson B. M., Vestergaard M., 2013, ApJ, 775, 60

Everett J. E., 2005, ApJ, 631, 689

Ferrarese L., Merritt D., 2000, ApJ, 539, L9

Gallagher S. C., Everett J. E., Abado M. M., Keating S. K., 2015, MNRAS, 451, 2991

Gaskell C. M., 1982, ApJ, 263, 79

Gavignaud I. et al., 2008, A&A, 492, 637

Gebhardt K. et al., 2000, ApJ, 539, L13

Greene J. E., Ho L. C., 2005, ApJ, 630, 122

Hewett P. C., Wild V., 2010, MNRAS, 405, 2302

Higginbottom N., Proga D., 2015, ApJ, 807, 107

Jarvis M. J., McLure R. J., 2006, MNRAS, 369, 182

Kaspi S., Smith P. S., Netzer H., Maoz D., Jannuzi B. T., Giveon U., 2000, ApJ, 533, 631

Kaspi S., Brandt W. N., Maoz D., Netzer H., Schneider D. P., Shemmer O., 2007, ApJ, 659, 997

Kelly B. C., Shen Y., 2013, ApJ, 764, 45

Kelly B. C., Vestergaard M., Fan X., Hopkins P., Hernquist L., Siemiginowska A., 2010, ApJ, 719, 1315

King A., Pounds K., 2015, ARA&A, 53, 115

King A. L. et al., 2015, MNRAS, 453, 1701

Kollmeier J. A. et al., 2006, ApJ, 648, 128

Konigl A., Kartje J. F., 1994, ApJ, 434, 446

Kormendy J., Ho L. C., 2013, ARA&A, 51, 511

Kratzer R. M., Richards G. T., 2015, AJ, 149, 61

Krawczyk C. M., Richards G. T., Mehta S. S., Vogeley M. S., Gallagher S. C., Leighly K. M., Ross N. P., Schneider D. P., 2013, ApJS, 206, 4

Lawrence A. et al., 2007, MNRAS, 379, 1599

Leighly K. M., 2004, ApJ, 611, 125

Luo B. et al., 2015, ApJ, 805, 122

McGill K. L., Woo J.-H., Treu T., Malkan M. A., 2008, ApJ, 673, 703

McLure R. J., Jarvis M. J., 2002, MNRAS, 337, 109

Maddox N., Hewett P. C., Péroux C., Nestor D. B., Wisotzki L., 2012, MNRAS, 424, 2876

Marziani P., Zamanov R. K., Sulentic J. W., Calvani M., 2003, MNRAS, 345, 1133

Marziani P., Martínez Carballo M. A., Sulentic J. W., Del Olmo A., Stirpe G. M., Dultzin D., 2016, Ap&SS, 361, 29

Mejia-Restrepo J. E., Trakhtenbrot B., Lira P., Netzer H., Capellupo D. M., 2016, MNRAS, 460, 187

Murray N., Chiang J., Grossman S. A., Voit G. M., 1995, ApJ, 451, 498

Onken C. A., Kollmeier J. A., 2008, ApJ, 689, L13

Onken C. A., Peterson B. M., 2002, ApJ, 572, 746

Pâris I. et al., 2014, A&A, 563, A54

Pâris I. et al., 2016, A&A, in press

Park D., Woo J.-H., Denney K. D., Shin J., 2013, ApJ, 770, 87

Peterson B. M., 1993, PASP, 105, 247

Peterson B. M., 2010, in Peterson B. M., Somerville R. S., Storchi-Bergmann T., eds, Proc. IAU Symp. 267, Co-Evolution of Central Black Holes and Galaxies. Kluwer, Dordrecht, p. 151

Peterson B. M., 2014, Space Sci. Rev., 183, 253

Peterson B. M. et al., 2004, ApJ, 613, 682

Plotkin R. M. et al., 2015, ApJ, 805, 123

Proga D., Stone J. M., Kallman T. R., 2000, ApJ, 543, 686

Rafiee A., Hall P. B., 2011, ApJS, 194, 42

Richards G. T., 2006, preprint (arXiv:e-prints)

Richards G. T., Vanden Berk D. E., Reichard T. A., Hall P. B., Schneider D. P., SubbaRao M., Thakar A. R., York D. G., 2002, AJ, 124, 1

Richards G. T. et al., 2006a, AJ, 131, 2766

Richards G. T. et al., 2006b, ApJS, 166, 470

Richards G. T. et al., 2011, AJ, 141, 167

Ross N. P. et al., 2013, ApJ, 773, 14

Runnoe J. C., Brotherton M. S., Shang Z., Wills B. J., DiPompeo M. A., 2013a, MNRAS, 429, 135

Runnoe J. C., Brotherton M. S., Shang Z., DiPompeo M. A., 2013b, MNRAS, 434, 848

Runnoe J. C., Brotherton M. S., DiPompeo M. A., Shang Z., 2014, MNRAS, 438, 3263

Schneider D. P. et al., 2010, AJ, 139, 2360

Shen Y., 2013, Bull. Astron. Soc. India, 41, 61

Shen Y., 2016, ApJ, 817, 55

Shen Y., Ho L. C., 2014, Nature, 513, 210

Shen Y., Liu X., 2012, ApJ, 753, 125

Shen Y., Greene J. E., Strauss M. A., Richards G. T., Schneider D. P., 2008, ApJ, 680, 169

Shen Y. et al., 2011, ApJS, 194, 45

Shen Y. et al., 2015, ApJS, 216, 4

Sulentic J. W., Marziani P., Dultzin-Hacyan D., 2000a, ARA&A, 38, 521

Sulentic J. W., Zwitter T., Marziani P., Dultzin-Hacyan D., 2000b, ApJ, 536, L5

Sulentic J. W., Repetto P., Stirpe G. M., Marziani P., Dultzin-Hacyan D., Calvani M., 2006, A&A, 456, 929

Sulentic J. W., Bachev R., Marziani P., Negrete C. A., Dultzin D., 2007, ApJ, 666, 757

Tilton E. M., Shull J. M., 2013, ApJ, 774, 67

Trakhtenbrot B., Netzer H., 2012, MNRAS, 427, 3081

van der Marel R. P., Franx M., 1993, ApJ, 407, 525

Vestergaard M., 2002, ApJ, 571, 733

Vestergaard M., 2004, ApJ, 601, 676

Vestergaard M., Osmer P. S., 2009, ApJ, 699, 800

Vestergaard M., Peterson B. M., 2006, ApJ, 641, 689

Vestergaard M., Fan X., Tremonti C. A., Osmer P. S., Richards G. T., 2008, ApJ, 674, L1

Wang H., Xing F., Zhang K., Wang T., Zhou H., Zhang S., 2013, ApJ, 776, L15

Wang J.-G. et al., 2009, ApJ, 707, 1334

Wu X.-B., Wang R., Kong M. Z., Liu F. K., Han J. L., 2004, A&A, 424, 793

York D. G. et al., 2000, AJ, 120, 1579

Zhang S., Wang H., Wang T., Xing F., Zhang K., Zhou H., Jiang P., 2014, ApJ, 786, 42

This paper has been typeset from a TeX/LaTeX file prepared by the author.